

Nighttime measurements of HO_x during the RONOCO project and analysis of the sources of HO₂

H.M. Walker et al.

We would like to thank the reviewers for their constructive comments which have helped to improve the manuscript. We have modified the manuscript in a number of areas, as suggested by the reviewers, and provide detailed responses to the comments below. The reviewers' comments are given in italics. Changes to the manuscript are given in red.

Review #1

1.1

The authors should clarify throughout the manuscript that their measurements of HO₂ include a small interference from RO₂ radicals and should be labeled as HO₂ rather than HO₂ to avoid confusion, including Figures 4, 7, 8, and 15. This would also be consistent with the presentation of their data (as HO₂*) in Stone et al. (2014b).*

We acknowledge that the measurements should be labelled HO₂*. The manuscript has been changed accordingly. HO₂* is defined on page 3009, and HO₂ measurements are referred to as HO₂* thereafter. Tables 4 and 5, and Figures 4, 7, 8, and 15 and their captions have been updated.

1.2 Pages 3008-3009

Although the RO₂ interference with HO₂ measurements has been quantified in the ground based instruments as described in Whalley et al. (2013), it appears that this has yet to be done for the aircraft instrument with only the interference due to ethene quantified and the rest calculated using the MCM. What was the distribution and calculated detection efficiencies of the different peroxy radicals calculated for the campaign conditions that led to the conclusion that only 15% of RO₂ radicals were detected by their instrument?

Whalley et al. (2013) describe in detail interference tests for three FAGE cells of varying design, one of which is comparable to that used in the aircraft measurements described in this work. In addition, interference tests have been conducted specifically for the aircraft FAGE instrument for ethene-derived peroxy radicals and are given by Stone et al. (2014). The

results of Whalley et al. indicate that the chemistry responsible for the observed interferences is well described by the MCM. MCM-based models are able to reproduce the observed interferences once the interference has been characterised for a single peroxy radical, since the level of interference is dependent on the efficiency of mixing of NO into the sampled air and the residence time of the sampled air in the FAGE cell. Both of these parameters are constrained in the model from experiment. Accordingly, the interferences presented in this work, as described by Stone et al. (2014), are determined relative to that for the ethene-derived peroxy radical using known chemistry.

The interference from the ethene-derived peroxy radical was determined experimentally, and was found to be (39.7 ± 4.8) % for a 1:1 mixture of HO₂ and RO₂. Stone et al. used a box model constrained to the temperature, pressure, and [NO] in the aircraft FAGE detection cell, with a detailed MCM-based chemistry scheme, to calculate the potential RO₂-based interference in the RONOCO HO₂ measurements. The model run time was varied until the model-predicted interference from ethene-derived RO₂ radicals was equal to the experimentally determined interference, thereby tuning the model to the conversion efficiency of HO₂ to OH. The model was initialised with equal concentrations of HO₂ and RO₂ so that an interference factor, f (i.e. the fractional increase in 'HO₂' signal upon addition of RO₂ to the system), could be calculated for every RO₂ species in the model. The greatest interference was calculated to come from isoprene-derived RO₂ (e.g. 57 % from HC(O)C(O)O₂), followed by RO₂ species derived from aromatic compounds and C₂ to C₅ alkenes.

The interference factors were applied to model-predicted RO₂ speciation and concentrations for the RONOCO flights. Model-predicted RO₂ species were dominated by CH₃O₂ (33 %; $f = 1.1$ %) and HO₂ (24 %; $f = 0.0$ %), with smaller contributions from RO₂ derived from *iso*-butene (12 %; $f = 0.5$ %), *cis*-2-butene and *trans*-2-butene (10 %; $f = 0.05$ %), and isoprene (2 %; $f = 7.6$ %). RO₂ species with high interference factors are a minor component of the total RO₂.

A plot of modelled HO₂ (no interference) vs modelled HO₂* (HO₂ + f^* RO₂) was best described by $\text{HO}_2^* = [1.15 \times \text{HO}_2] + 2 \times 10^5 \text{ cm}^{-3}$. The potential interference in the FAGE measurements of HO₂ during RONOCO was calculated using this equation.

The following sentences have been added to the manuscript to clarify the discussion:

P3008 L18:

“Whalley et al. (2013) show that the chemistry responsible for the observed interferences is well known, and that a model using the Master Chemical Mechanism (MCM, version 3.2: Jenkin et al., 1997; Saunders et al., 2003; Bloss et al., 2005, via <http://mcm.leeds.ac.uk/MCM>) can reproduce the interferences once tuned to the conversion efficiency of HO₂ to OH in the FAGE detection cell. Accordingly, Stone et al. (2014b) have applied the results of the ethene-derived RO₂ interference testing in a modelling study to assess the effect of the interference on the HO₂ measurements made during the RONOCO and SeptEx campaigns.”

P3008 L25:

“The model run time was varied until the model-predicted interference from ethene-derived RO₂ radicals was equal to the experimentally determined interference, thereby tuning the model to the conversion efficiency of HO₂ to OH.”

P3009 L8:

“The interference factors were applied to model-predicted RO₂ speciation and concentrations for the RONOCO flights. Model-predicted RO₂ species were dominated by CH₃O₂ (33 %; $f = 1.1$ %) and HO₂ (24 %; $f = 0.0$ %), with smaller contributions from RO₂ derived from *iso*-butene (12 %; $f = 0.5$ %), *cis*-2-butene and *trans*-2-butene (10 %; $f = 0.05$ %), and isoprene (2 %; $f = 7.6$ %). RO₂ species with high interference factors were a minor component of the total RO₂.”

1.3 Page 3011

The authors state that the LOD reported in Table 4 are for an averaging time of 1 min, while on pages 3007-3008 a 5 min time average is state for these LOD. Stone et al. (2014b) lists these LODs for 4-5 min averages.

We thank the reviewers for highlighting this inconsistency. The averaging time is 5 minutes. The averaging time has been included in the table caption to make it clearer, and the main text has been changed as follows:

P3011 L27:

“Table 4 summarises the OH and HO₂* measurements during RONOCO and SeptEx and gives the instrument’s average 1 σ limit of detection **for a 5 minute averaging period.**”

1.4 Page 3014

The authors present the OH and HO₂ measurements as a function of altitude, but calculate what appear to be average rates in Figures 11-14. This should be clarified in the text. Did the authors observe an altitude dependence of these rates? A figure that illustrates the measured concentrations of ozone, NO₃ and alkenes as a function of altitude would be useful.

Average rates of production are presented in Figures 11 to 14. This has been made clearer in the text:

P3017, L12: “The rates of reaction and rates of instantaneous production of HO₂ presented hereafter are average values for individual flights, seasons, or times of day.”

The figure captions for Table 6 and Figures 11-14 have been amended to read “average rates of reaction” or “average rates of instantaneous production of HO₂” as appropriate.

No significant altitude dependence of the rates of reaction of O₃ and NO₃ with the alkenes measured, or of the rate of production of HO₂, was observed.

A figure illustrating the altitude profiles of NO₃, O₃ and two selected alkenes (*trans*-2-butene and propene, which are dominant in reactions of oxidants with the alkenes measured during RONOCO, and in production of HO₂) is shown below (Figure 1) and will be included in the manuscript as Figure 3 (numbering of subsequent figures and references to them have been updated).

The new figure is introduced:

P3006 L19:

“Table 3 also highlights the unusual chemical conditions encountered during flight B537 on 20th July 2010, discussed further in Sect. 4.1. Nighttime altitude profiles of NO₃, O₃, *trans*-2-butene, and propene (the latter two being illustrative of the alkenes measured) are given in Fig. 3.”

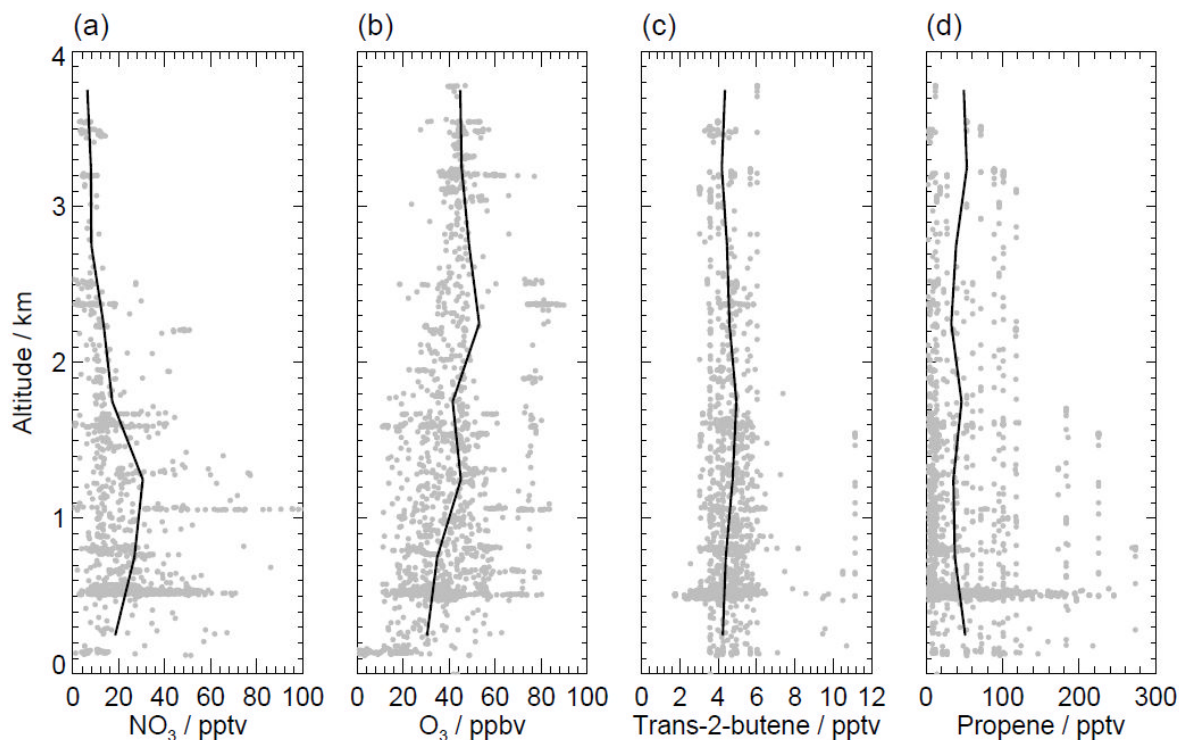


Figure 1. Nighttime altitude profiles of a) NO_3 ; b) O_3 ; c) Trans-2-butene; d) Propene, showing 60 second data (grey points) and mean values in 500 m altitude bins (solid black lines).

Review #2

2.1 P2999 L21

The oxidising capacity of the atmosphere is described as its “ability” to remove trace gases. While capacity is a physical and quantifiable characteristic of a system, ability is not. Please reword.

The authors acknowledge that “ability” is not suitable. The sentence contributes nothing further to the preceding sentence, so it has been removed.

2.2 P3008 L23-26

Why were equal concentrations of HO_2 and RO_2 used to constrain the model? The sentence “the model was run until the model interference ... matched the interference measured in the

interference experiments” is clumsy. Please re-word and state how the model was tuned to get it to match.

Equal concentrations of HO₂ and RO₂ were used to initialise the model calculations used to determine RO₂ interferences. The experimental determination of RO₂ interference used equal concentrations of HO₂ and RO₂, and compared the ‘HO₂’ signal to experiments in which no RO₂ radicals were present. The fractional increase in the observed signal on addition of RO₂ to the system thus represents the fractional RO₂ interference. The model calculations were performed to replicate the experimental method, with the model tuned to the observed increase in ‘HO₂’ signal on inclusion of the RO₂ species by varying the reaction time (representing the extent of mixing of NO and residence time in the detection cell) until the modelled interference matched the experimental observations.

The sentence has been reworded as follows:

P3008 L25 to P3009 L1:

“The model run time was varied until the model-predicted interference from ethene-derived RO₂ radicals was equal to the experimentally-determined interference, thereby tuning the model to the conversion efficiency of HO₂ to OH.”

Please see Sect 2.1.2 for further discussion of this section of the manuscript.

2.3 P3008 L28

“interference measurements described above”. There is no description of the so-called interference experiments, only a citation to Whalley.

The sentence has been changed (see Sect. 1.6 of this document), and “interference measurements described above” has been removed. The aircraft instrument experiments, which have not been published elsewhere, are mentioned briefly after the reference to Whalley et al.

2.4 P3009 L14

After describing the corrections for HO₂ and deriving alkene dependent correction factors for the HO₂ measurements the authors then state that the correction (on average 14 %) was not made. If they trust the correction, they should apply it to the data.

Correction of the observations of HO₂* to determine HO₂ relies on the model calculated RO₂ speciation and RO₂ concentrations, and would thus make HO₂ a combination of observations and model products. In order to avoid this we report the HO₂* as observed, as is the case for other groups (e.g. Lu et al., 2012; Griffith et al., 2013), and apply the interference to the modelled HO₂ (as described in Stone et al., 2014), maintaining independence of the observed data from the modelled data.

The manuscript has been changed as follows:

P3009 L14:

“The HO₂ measurements made during RONOCO and SeptEx were not adjusted since speciated RO₂ measurements were not available. The measurements are hereafter referred to as HO₂*.”

2.5 P3011 L10

Wall losses of NO₃ and N₂O₅ were determined prior to and after each flight. What was the variability in this parameter and how large the correction factor? The total uncertainty in the NO₃ measurement is given as 11 %. This seems too low, especially considering that the NO₃-transmission of the aircraft inlet is unknown.

As described in detail by Kennedy et al. (2011) potential changes to the transmission efficiency caused by ageing or build-up of particulates on the PFA surface were investigated by determining the pseudo first order loss rate of NO₃ onto the instrument's internal surface, $k_{\text{NO}_3 \text{ loss}}$, prior to and following each flight. For each flight the measured rate coefficient was found to equal that measured in the laboratory ($0.27 \text{ s}^{-1} \pm 0.02 \text{ s}^{-1}$), within error, indicating negligible change to the PFA surface.

High flow rates through channels 1 and 2 ensure short residence times (380 ms in channel 1 and 170 ms in channel 2). The calculated transmission efficiencies of NO₃ into channels 1 and 2 are $T_1 = 90 \% \pm 1.5 \%$ and $T_2 = 96 \% \pm 0.7 \%$, respectively.

The transmission efficiency of N₂O₅ into channel 1, T_0 , depends upon direct loss of N₂O₅ to the walls of the inlet and wall losses of NO₃ produced by thermal dissociation. The loss rate of N₂O₅ to the walls of the inlet was found to be considerably slower than that for NO₃ ($k_{\text{N}_2\text{O}_5 \text{ loss}} = 0.042 \text{ s}^{-1} \pm 0.004 \text{ s}^{-1}$). The short residence time in the inlet (<0.02 s) ensures that direct losses of N₂O₅ are within the error of ambient N₂O₅ measurements and can be

neglected. Accordingly T_0 is determined by loss of NO_3 following thermal dissociation. For a residence time of 250 ms between the preheater and the detection cell T_0 is calculated to be equal to $93 \% \pm 6 \%$.

The manuscript has been changed as follows:

“In addition, wall losses of NO_3 and N_2O_5 were determined before and after each flight to account for changes in the surface properties of the inlet and detection cell walls, **which were found to be negligible.**”

2.6 P3015 L17

Is the value of 0.6 (equation5) valid for all VOCs ? The authors should consider giving some examples of F_{RO} for a few different alkenes.

The calculation follows the method employed in the MCM, a near-explicit state-of-the-art organic chemistry mechanism, in which each peroxy radical is assumed to react with all other peroxy radicals at a single, collective rate. The branching ratios to RO, RC(O)CH_3 , and RCH_2OH , and ROH, are determined by the structure of the peroxy radical. The value of 0.6 for primary and secondary RO_2 (excluding CH_3O_2 , see below) is based on the mean of the values of the self-reactions of $\text{C}_2\text{H}_5\text{O}_2$, *i*- $\text{C}_3\text{H}_7\text{O}_2$, *neo*- $\text{C}_5\text{H}_{11}\text{O}_2$, *c*- $\text{C}_5\text{H}_{11}\text{O}_2$, $\text{CH}_2=\text{CHCH}_2\text{O}_2$, $\text{HOCH}_2\text{CH}_2\text{O}_2$, $\text{CH}_3\text{OCH}_2\text{O}_2$, $\text{CH}_3\text{C(O)CH}_2\text{O}_2$, and $\text{CH}_2\text{ClCH}_2\text{O}_2$, which range between 0.5 and 0.75, and is the best estimate using currently-available data. Nitrooxyalkyl peroxy radicals are assumed to react in the same manner as the RO_2 species listed above. CH_3O_2 is treated separately in the MCM, with a branching ratio of 0.330 to the non-terminating (RO) channel. Note that Equation 5 refers to the reactions of nitrooxyalkyl peroxy radicals produced from NO_3 + alkene reactions, and therefore does not include CH_3O_2 , which is produced in the reactions of O_3 with alkenes.

Some examples of F_{RO} have been given in the manuscript as follows:

P3015 L18:

“where RO_2 represents all peroxy radicals. **Average values of F_{RO} for the NO_3 + alkene reactions range between 0.50 for *trans*-2-pentene- and 1-pentene-derived RO_2 species and 0.61 for ethene-derived RO_2 species.**”

P3016 L19:

“... F_{RO} is the fraction of RO_2 radicals that react to produce RO radicals, and F_{HO_2} is the fraction of RO radicals that react to produce HO_2 radicals, which is equal to 1 for all the alkenes studied. Average values of F_{RO} for the $O_3 +$ alkene reactions range between 0.54 for 1-pentene-derived RO_2 species and 0.64 for 1-butene- and *trans*-2-pentene-derived RO_2 species.”

2.7 P3017 L24

“the seasonal difference in NO_3 concentrations may have been the result of lower temperatures.” As the temperatures, the equilibrium constants and NO_2 levels are known this statement can be confirmed and quantified.

We have calculated $K_{eq}[NO_2] = [N_2O_5]/[NO_3]$ for summer and winter:

$$K_{eq}[NO_2]_{summer} = 4.8$$

$$K_{eq}[NO_2]_{winter} = 29.6$$

$$[N_2O_5]/[NO_3]_{summer} = 3.4$$

$$[N_2O_5]/[NO_3]_{winter} = 18.1$$

Though $K_{eq}[NO_2]$ is not equal to $[N_2O_5]/[NO_3]$ in either season, both $K_{eq}[NO_2]$ and $[N_2O_5]/[NO_3]$ increase between summer and winter, supporting the hypothesis that the decreased concentrations of NO_3 during winter are attributable to the change in the N_2O_5 - NO_3 equilibrium.

The manuscript has been changed to reflect this:

P3017 L24 to P3018 L1:

“This seasonal difference in NO_3 concentrations is attributable to the lower mean nighttime temperature in winter (277.7K) compared to summer (286.7 K) which disfavours NO_3 in the thermal equilibrium $N_2O_5 \rightleftharpoons NO_3 + NO_2$. $K_{eq}[NO_2]$, which determines $[N_2O_5]/[NO_3]$, is calculated to be 4.8 in summer and 29.6 in winter.”

2.8 P3021

The authors calculate the rate of HO_2 production assuming that the losses of NO_3 are completely accounted for by the alkenes measured. Based on this assumption, the authors should also be able to calculate the steady-state mixing ratios of NO_3 as the production term (via O_3 and NO_2) is known. They will find that the NO_3 concentrations calculated this way

are too high as the true overall loss rate is actually not known. Indeed on page 3023 the authors show that the model used also over-predicts NO₃. The authors then state that the discrepancy between modelled and measured NO₃ helps to explain the model overprediction of the role of NO₃ in HO₂ generation. I'm not sure if this is correct. If the model does not account for the losses of NO₃ with hydrocarbons that were not measured it will generate more N₂O₅ (as the model NO₃ lifetime increases) and thus underestimate the rate of oxidation of VOCs by NO₃ and thus also UNDERpredict the rate of RO₂ production.

We acknowledge that calculating steady-state mixing ratios of NO₃ using NO₃ + alkenes as the sole loss mechanism would indeed lead to overprediction of NO₃ concentrations compared to the measured values. However, we aim to highlight the relative importance of NO₃ and O₃ in the production of HO₂ during summer and winter, and to compare the calculations to the results of the modelling study by Stone et al. (2014), rather than focussing on the absolute rates of production of HO₂. Both the modelling study and the current work use observed values of [O₃] to calculate rates of reaction between O₃ and alkenes and subsequent rates of production of HO₂, so the contribution of O₃ + alkenes to production of HO₂ is equivalent in Stone et al. and in the current work. Since the model overpredicts the observed NO₃ concentrations by 80 % on average, and is constrained to observed values of [O₃], the model is expected to predict an enhanced role for NO₃ relative to that of O₃ in production of HO₂, compared to calculations based entirely on the observations.

The manuscript has been changed to highlight the relative importance of NO₃ and O₃ in production of HO₂:

P3024, L6 to L12:

“These results are in general agreement with the results of the analysis presented in Sect. 6.1, though the model predicts a more important role for NO₃ (80 % of RO_x radical production, **which is 7.2 times the contribution from O₃ + alkenes**) than is predicted by the analysis based on the observations (69 % of HO₂ radical production during summer, **which is 2.1 times the contribution from O₃ + alkenes**). **The model predicts a relatively small role for O₃ in both summer and winter.** The model is constrained to measured values of O₃, but overpredicts NO₃....”

2.9 P3023 L15

Data from flight B537 were excluded owing to atypical observations of HO₂, NO₃, O₃ and “other chemical species”. What does atypical mean? Sometimes “atypical” events can be a better test of our understanding of chemical processes than analysis of only the data that we a priori expect to find.

In this instance atypical refers to the high concentrations of HO₂, NO₃, O₃, CO, aerosol surface area, and aerosol organic fraction compared to the values measured in other flights, as described in Sect. 4.1 (P3013, L5 to L10). We agree that this flight offers a good opportunity to investigate the atmospheric chemistry sampled, which is why we have used it as a small case study in the current work, highlighting the observed correlation between HO₂* and NO₃ and including the analysis of the production of HO₂ during this individual flight. Model results constrained to measurements of long-lived species made during flight B537 were found to be outliers from the rest of the data, and were excluded to enable analysis of the data without the influence of this flight. A modelling study dedicated to interpreting the chemistry observed during B537 would be valuable.

2.10 P3026 L29

“and others” is not a useful reference.

The reference has been changed to include other publications, and “and others” has been removed:

“Alkene ozonolysis also plays a significant role in nocturnal oxidation in agreement with Salisbury et al. (2001), Geyer et al. (2003), Ren et al. (2003a), Emmerson et al. (2005), Ren et al. (2006), and Volkamer et al. (2010).”

References

Griffith, S. M., Hansen, R. F., Dusanter, S., Stevens, P. S., Alaghmand, M., Bertman, S. B., Carroll, M. A., Erickson, M., Galloway, M., Grossberg, N., Hottle, J., Hou, J., Jobson, B. T., Kammrath, A., Keutsch, F. N., Lefer, B. L., Mielke, L. H., O’Brien, A., Shepson, P. B., Thurlow, M., Wallace, W., Zhang, N., and Zhou, X. L.: OH and HO₂ radical chemistry during PROPHET 2008 and CABINEX 2009 – Part 1: Measurements and model comparison, Atmos. Chem. Phys, 13, 5403-5423, 2013.

Lu, K. D., Rohrer, F., Holland, F., Fuchs, H., Bohn, B., Brauers, T., Chang, C. C., Häsel, R., Hu, M., Kita, K., Kondo, Y., Li, X., Lou, S. R., Nehr, S., Shao, M., Zeng, L. M., Wahner, A., Zhang, Y. H., Hofzumahaus, A.: Observation and modelling of OH and HO₂ concentrations in the Pearl River Delta 2006: a missing OH source on a VOC rich atmosphere, *Atmos. Chem. Phys.*, 12, 1541-1569, 2012.

1 **Nighttime measurements of HO_x during the RONOCO**
2 **project and analysis of the sources of HO₂**

3

4 **H.M. Walker¹, D. Stone¹, T. Ingham^{1,2}, S. Vaughan¹, B. Bandy³, M. Cain^{4,5}, R.L.**
5 **Jones⁴, O.J. Kennedy⁴, M. McLeod⁴, B. Ouyang⁴, J. Pyle^{4,5}, S. Bauguitte^{6,7}, G.**
6 **Forster^{8,9}, M.J. Evans^{10,11}, J.F. Hamilton¹⁰, J.R. Hopkins^{10,11}, J.D. Lee^{10,11}, A.C.**
7 **Lewis^{10,11}, R.T. Lidster¹⁰, S. Punjabi^{10,11}, W.T. Morgan^{12,13}, D.E. Heard^{1,2}**

8

9 [1] {School of Chemistry, University of Leeds, Leeds, UK}

10 [2] {National Centre for Atmospheric Science, University of Leeds, Leeds, UK}

11 [3] {School of Environmental Sciences, University of East Anglia, Norwich, UK}

12 [4] {Department of Chemistry, University of Cambridge, Cambridge, UK}

13 [5] {National Centre for Atmospheric Science, University of Cambridge, Cambridge, UK}

14 [6] {Facility for Airborne Atmospheric Measurements (FAAM), Cranfield University,
15 Cranfield, UK}

16 [7] {National Centre for Atmospheric Science, FAAM, Cranfield University, Cranfield, UK}

17 [8] {Centre for Ocean and Atmospheric Sciences, School of Environmental Sciences,
18 University of East Anglia, Norwich, UK}

19 [9] {National Centre for Atmospheric Science, University of East Anglia, Norwich, UK}

20 [10] {Wolfson Atmospheric Chemistry Laboratories, Department of Chemistry, University of
21 York, York, UK}

22 [11] {National Centre for Atmospheric Science, University of York, York, UK}

23 [12] {School of Earth, Atmospheric and Environmental Sciences, University of Manchester,
24 Manchester, UK}

25 [13] {National Centre for Atmospheric Science, University of Manchester, Manchester, UK}

26

27 Correspondence to: D. E. Heard (d.e.heard@leeds.ac.uk)

28

29 **Abstract**

30 Measurements of the radical species OH and HO₂ were made using the Fluorescence Assay
31 by Gas Expansion (FAGE) technique during a series of nighttime and daytime flights over
32 the UK in summer 2010 and winter 2011. OH was not detected above the instrument's 1σ
33 limit of detection during any of the nighttime flights or during the winter daytime flights,
34 placing upper limits on [OH] of 1.8 × 10⁶ molecule cm⁻³ and 6.4 × 10⁵ molecule cm⁻³ for the
35 summer and winter flights, respectively. HO₂ reached a maximum concentration of 3.2 × 10⁸
36 molecule cm⁻³ (13.6 pptv) during a nighttime flight on 20th July 2010, when the highest
37 concentrations of NO₃ and O₃ were also recorded. Analysis of the rates of reaction of OH, O₃,
38 and the NO₃ radical with measured alkenes indicates that the summer nighttime troposphere
39 can be as important for the processing of VOCs as the winter daytime troposphere. Analysis
40 of the instantaneous rate of production of HO₂ from the reactions of O₃ and NO₃ with alkenes
41 has shown that, on average, reactions of NO₃ dominated nighttime production of HO₂ during
42 summer, and reactions of O₃ dominated nighttime HO₂ production during winter.

43

44 **1 Introduction**

45 Trace gases emitted into the atmosphere, including pollutants and greenhouse gases, are
46 removed primarily by oxidation. The hydroxyl radical, OH, is the most important oxidising
47 species in the daytime troposphere, reacting with numerous species including volatile organic
48 compounds (VOCs), CO, SO₂, and long-lived anthropogenic halogenated compounds. ~~The
49 oxidising capacity of the atmosphere, that is its ability to remove trace gases, is determined
50 by the concentration of OH.~~ During the day, primary production of OH (i.e. initialisation of
51 the radical chain) occurs predominantly via photolysis of ozone at λ ≤ 340 nm followed by
52 reaction of the resulting electronically excited oxygen atom, O(¹D), with water vapour. The
53 OH-initiated oxidation of VOCs leads to the production of the hydroperoxy radical, HO₂, and
54 together the two radicals form the HO_x family. A key reaction in the conversion of OH to
55 HO₂ is the reaction with CO:

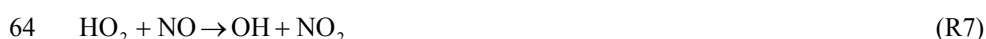


58 Reaction of OH with VOCs results in the production of organic peroxy radicals, RO₂:

Comment [HW1]: See reviewers' comments Sect 2.1



61 Reactions of HO_2 and RO_2 with NO propagate the HO_x radical chain, regenerating OH :



65 The production of OH through photolysis of ozone (and other species at longer wavelengths)
66 is limited to daylight hours, and oxidation of trace gases at night proceeds through alternative
67 mechanisms. Two mechanisms are known to initiate HO_x radical chemistry and oxidation
68 chemistry at night: ozonolysis of alkenes, and reactions of the nitrate radical, NO_3 , with
69 alkenes.

70 Reactions of ozone with alkenes occur via addition of ozone to the double bond to form a
71 five-membered ring called a primary ozonide. The primary ozonide decomposes to form one
72 of two possible pairs of products, each pair consisting of a carbonyl compound and a
73 vibrationally- and rotationally-excited carbonyl oxide termed a Criegee intermediate (CI).
74 The simplest gas-phase CI, CH_2OO , and the alkyl-substituted CH_3CHOO , have been
75 observed directly by photoionisation mass spectrometry (Taatjes et al., 2008; Beames et al.,
76 2012; Taatjes et al., 2012; Welz et al., 2012; Beames et al., 2013; Taatjes et al., 2013; Stone
77 et al., 2014a), by infrared absorption spectroscopy (Su et al., 2013), and by microwave
78 spectroscopy (Nakajima and Endo, 2013, 2014). Excited CIs may be stabilised by collision
79 with surrounding molecules (Donahue et al., 2011; Drozd and Donahue, 2011), or may
80 undergo isomerisation or decomposition to yield products including OH , H , and subsequently
81 HO_2 (Paulson and Orlando, 1996; Kroll et al., 2001a; Kroll et al., 2001b; Kroll et al., 2002;
82 Johnson and Marston, 2008). Stabilised CIs (SCIs) are known to react with a variety of
83 compounds, including H_2O , NO_2 , SO_2 , and a variety of organic compounds (e.g. Mauldin III
84 et al., 2012; Taatjes et al., 2012; Ouyang et al., 2013; Taatjes et al., 2013; Stone et al., 2014a;
85 Taatjes et al., 2014). There is experimental evidence for the formation of OH from thermal
86 decomposition of SCIs, on a much longer timescale than the decomposition or isomerisation
87 of excited CIs (Kroll et al., 2001a; Kroll et al., 2001b). The OH produced through these
88 ozonolysis mechanisms will proceed to oxidise other VOC species. Criegee intermediates
89 formed in the ozonolysis of alkenes are known to be an important source of HO_x during the

90 day and at night (Paulson and Orlando, 1996; Donahue et al., 1998; Kanaya et al., 1999;
91 Salisbury et al., 2001; Geyer et al., 2003; Ren et al., 2003a; Heard et al., 2004; Harrison et al.,
92 2006; Ren et al., 2006; Sommariva et al., 2007). The gas-phase ozonolysis of unsaturated
93 VOCs, and in particular the role and subsequent chemistry of the Criegee intermediate, have
94 been reviewed in detail by Johnson and Marston (2008), Donahue et al. (2011), Vereecken
95 and Francisco (2012), and Taatjes et al. (2014).

96 Another key nighttime oxidant, NO₃, is formed primarily by reaction of NO₂ with ozone.
97 NO₃ reacts with a range of species in the troposphere, and its reaction with alkenes is known
98 to be an important nighttime oxidation mechanism (Salisbury et al., 2001; Geyer et al., 2003;
99 Sommariva et al., 2007; Emmerson and Carslaw, 2009; Brown et al., 2011). The reaction
100 between NO₃ and an alkene proceeds primarily via addition to a double bond, to form a
101 nitrooxyalkyl radical, R-ONO₂. At atmospheric pressure, the main fate of the nitrooxyalkyl
102 radical is reaction with O₂ (Berndt and Böge, 1994) to produce a nitrooxyalkyl peroxy
103 radical, O₂-R-ONO₂. The nitrooxyalkyl peroxy radical can react with NO₂, HO₂, RO₂, NO
104 and NO₃, of which the latter two reactions lead to formation of the nitrooxyalkoxy radical,
105 O-R-ONO₂. The nitrooxyalkoxy radical can undergo isomerisation, decomposition, or
106 reaction with O₂. Reaction with O₂, analogous to the reaction of organic alkoxy radicals,
107 yields HO₂:



109 Thus, nighttime oxidation of hydrocarbons by NO₃ leads to production of HO₂. Reaction of
110 HO₂ with NO (Reaction (R7)), O₃ and NO₃ can generate OH:



113 Atkinson and Arey (2003) published a detailed review of tropospheric degradation of VOCs,
114 including reaction with O₃ and NO₃. A comprehensive review of nighttime radical chemistry
115 is given by Brown and Stutz (2012).

116 The oxidising capacity of the nocturnal troposphere is thought to be controlled by the
117 reactions described above, with a limited role for OH and HO₂ due to the absence of their
118 photolytic sources. Oxidation of VOCs at night can have significant effects on daytime air
119 quality and tropospheric ozone production (Brown et al., 2004; Brown et al., 2006; Wong and
120 Stutz, 2010; Brown et al., 2011). Several field measurement campaigns have involved
121 nighttime measurements of OH, HO₂, RO₂, and NO₃ (see Table 1), and have highlighted the

122 importance of the vertical profile of nighttime radical concentrations and chemistry (Geyer
123 and Stutz, 2004a, b; Stutz et al., 2004; Volkamer et al., 2010), but prior to the current work
124 there had been no aircraft-based studies of nighttime chemistry involving measurements of
125 both NO_3 and HO_2 , to enable vertical profiling of the lower atmosphere and full evaluation of
126 the nocturnal radical budget. Table 1 gives details of some previous measurements and
127 modelling of nighttime HO_x concentrations in polluted or semi-polluted environments.
128 Highlights from these studies are discussed here, with particular attention paid to those
129 involving measurements of HO_x , NO_3 , and O_3 , and in which the contributions made by O_3
130 and NO_3 to nighttime radical chemistry have been considered.

131 Geyer et al. (2003) report radical measurements and modelling from the 1998 Berliner Ozone
132 Experiment (BERLIOZ). Measurements of NO_3 , RO_2 , HO_2 and OH were made by matrix
133 isolation electron spin resonance (MIESR), chemical amplification (CA), and laser-induced
134 fluorescence (LIF) spectroscopy at a site approximately 50 km from Berlin. HO_2 was
135 detected at night with concentrations frequently as high as 5×10^7 molecule cm^{-3}
136 (approximately 2 pptv), and an average concentration of 1×10^8 molecule cm^{-3} over one hour
137 (02:00 to 03:00) of nocturnal measurements during an intensive period of the study (Holland
138 et al., 2003). OH was usually below the limit of detection of the LIF instrument
139 (3.5×10^5 molecule cm^{-3}). Modelling revealed that nitrate radical reactions with terpenes
140 were responsible for producing 53 % of HO_2 and 36 % of OH radicals in the night, with
141 ozonolysis accounting for production of the remaining 47 % of HO_2 and 64 % of OH
142 radicals. A positive linear correlation between RO_2 and NO_3 was observed and was
143 reproduced by the model.

144 Reactions of O_3 with alkenes were found to be responsible for the majority of formation of
145 OH during the winter PUMA (Pollution of the Urban Midlands Atmosphere) campaign (a
146 low photolysis urban environment) (Heard et al., 2004; Emmerson et al., 2005; Harrison et
147 al., 2006). Measurements of OH , HO_2 and RO_2 were unavailable at night, but model-
148 predicted values of these radicals were used to calculate that 90 % of nighttime initiation via
149 HO_2 was from O_3 reactions. Without measurements of NO_3 during the campaign, there was
150 no estimate of its contribution to radical initiation.

151 Modelling results from the MCMA-2003 (Mexico City) field campaign (Volkamer et al.,
152 2010) indicate that nighttime radical production at roof-top level (approximately 16 m above
153 the ground) was dominated by ozonolysis of alkenes, and that reactions of NO_3 with alkenes
154 played only a minor role. The measurement site was located in a polluted urban environment,

155 with high levels of NO, NO₂ and O₃. NO₃ was observed at a maximum concentration of 50
156 pptv during the night at a mean height above the ground of 70 m. Roof-top level
157 concentrations of NO₃ were estimated using a linear scaling factor calculated from the
158 observed O₃ vertical gradient, and were found to be, on average, 3 times lower than the
159 concentrations measured at 70 m. This predicted vertical gradient accounts for the relative
160 unimportance of NO₃ reactions in radical initiation at roof-top level. Propagation of RO₂
161 radicals to HO₂ and OH, by reaction with NO₃, was found to be negligible.

162 The 2006 Texas Air Quality Study (TexAQS) involved a series of nighttime flights onboard
163 the NOAA P-3 aircraft over Houston, Texas, and along the Gulf Coast (Brown et al., 2011).
164 Loss rates and budgets of NO₃ and highly reactive VOCs were calculated, but there were no
165 measurements of OH, HO₂ and RO₂ during the flights. Budgets for NO₃ show that it was lost
166 primarily through reactions with unsaturated VOCs, but the contribution to NO₃ loss through
167 reaction with peroxy radicals was uncertain because of the lack of direct measurements of
168 RO₂ during the flights. NO₃ dominated VOC oxidation, being 3 to 5 times more important
169 than O₃.

170 In summary, NO₃ and O₃ have both been found to dominate radical initiation in the nighttime
171 troposphere, and in some situations the two mechanisms were found to be equally important.
172 The relative importance of O₃- and NO₃-initiated oxidation depends on the availability of
173 NO₃, which is determined by the amount of NO_x present in the atmosphere and the ratio of
174 NO to NO₂, and the concentration and species distribution of VOCs (Bey et al., 2001; Geyer
175 et al., 2003). A modelling study by Bey et al. (2001) suggests that nocturnal radical initiation
176 is driven by alkene ozonolysis in urban environments or in environments with low NO_x
177 concentrations, while both O₃ and NO₃ contribute to radical initiation in rural environments
178 with moderate NO_x levels. It is expected that NO₃ dominates nocturnal radical initiation in air
179 masses containing sufficient NO₂ and O₃ for NO₃ production while being deprived of NO
180 (e.g. air masses downwind of urban areas). Geyer and Stutz (2004b) have found that the
181 effects of suppressed mixing in the nocturnal boundary layer can also control whether NO₃ or
182 O₃ dominates nighttime radical chemistry.

183 In this paper we report airborne measurements of OH and HO₂ made during the RONOCO
184 (ROle of Nighttime chemistry in controlling the Oxidising Capacity of the atmosphere) and
185 SeptEx (September Experiment) projects in 2010 and 2011. The rates of reaction between O₃,
186 NO₃, and OH with the alkenes measured during the flights are investigated. Analysis of
187 radical production from the nighttime reactions of O₃ and NO₃ with alkenes is also given.

188 Comparisons are made between the daytime and nighttime chemistry studied, and between
189 the summer and winter measurement periods. Details and results of a box modelling study,
190 and comparison to the observations, are given by Stone et al. (2014b).

191

192 **2 Details of the RONOCO and SeptEx fieldwork**

193 RONOCO is a NERC-funded consortium project aimed at improving our understanding of
194 the mechanisms and impact of nocturnal oxidation chemistry over the UK. The RONOCO
195 fieldwork consisted of two measurement campaigns, in July 2010 and January 2011. An
196 additional fieldwork period, SeptEx, was conducted in September 2010. The RONOCO and
197 SeptEx flights were conducted onboard the BAe-146 research aircraft operated by the Facility
198 for Airborne Atmospheric Measurements (FAAM). Both field measurement campaigns were
199 based at East Midlands Airport (52.8° N, 1.3° W) in the UK. During RONOCO the majority
200 of the flying took place at night, with occasional flights beginning or ending in daylight hours
201 to study chemical behaviour at dusk and dawn. Flights during SeptEx were mainly during the
202 day, providing a useful comparison to the nocturnal chemistry.

203 Flights were conducted between altitudes of 50 m and 6400 m, above the UK and the North
204 Sea. Figure 1 shows the flight tracks during the summer, SeptEx, and winter measurements
205 coloured by altitude. Measurements of OH and HO₂ were made using the University of Leeds
206 aircraft-based Fluorescence Assay by Gas Expansion (FAGE) instrument. A suite of
207 supporting measurements, including CO, O₃, NO, H₂O, VOCs, NO₃, and HCHO, were made
208 during the flights and have been used in the current work. Table 2 summarises the techniques
209 used to measure these species.

210 Air mass histories for each flight have been calculated using the UK Met Office Numerical
211 Atmospheric-dispersion Modelling Environment (NAME). NAME is a three-dimensional
212 Lagrangian particle dispersion model (Jones et al., 2007) which is run here using the UK
213 Meteorological Office's Unified Model meteorological fields. Model 'particles', restricted to
214 a 300 m deep layer from the surface, were released along the flight path and were tracked
215 backwards through the modelled atmosphere. Model particle densities were integrated over
216 24 h periods, beginning at 24, 48, 72, and 96 hours before each flight. The resulting
217 'footprint' maps show the regions where the measured air has been in contact with the
218 surface over the 4 days preceding a flight. An example is shown in Fig. 2, which shows
219 model particle densities integrated over the 24 hour period beginning 48 hours prior to flight

220 B535. The majority of the summer flights were characterised by air masses originating from
221 the west and south west of the UK, having Atlantic or continental European influences. The
222 SeptEx flights were predominantly influenced by air masses from the north-east, east, and
223 south-east of the UK, with northern European influences. The winter flights were mainly
224 characterised by air masses arriving from the west of the UK, bringing Atlantic influences.

225 Table 3 gives mean and maximum mixing ratios of CO, O₃, NO, and NO₂ measured during
226 RONOCO and SeptEx. The mean mixing ratios of NO measured during the summer
227 RONOCO flights are much lower than ground-based nighttime measurements (e.g. 1.0 ppbv
228 during TORCH (Emmerson and Carslaw, 2009), 0–20 ppbv during PMTACS-NY, (Ren et
229 al., 2006)), but are comparable with previous airborne nighttime measurements (e.g.
230 < 30 pptv during TexAQS (Brown et al., 2011)). Mean values of NO up to 14 pptv were
231 reported by Salisbury et al. (2001) for semi-polluted air masses sampled at Mace Head. These
232 comparisons indicate that the RONOCO and SeptEx flights enabled sampling of air masses
233 generally removed from the influence of NO in fresh surface emissions. Table 3 also
234 highlights the unusual chemical conditions encountered during flight B537 on 20th July 2010,
235 discussed further in Sect. 4.1. Nighttime altitude profiles of NO₃, O₃, *trans*-2-butene, and
236 propene (the latter two being illustrative of the alkenes measured) are given in Fig. 3.

Comment [HW2]: See Reviewers'
Comments Sect 1.4

237

238 3 Experimental

239 3.1 The Leeds FAGE aircraft instrument

240 The University of Leeds Aircraft FAGE instrument has been described in detail by Commane
241 et al. (2010). A brief description is given here. The instrument, which was designed
242 specifically for use onboard the FAAM BAe-146 research aircraft (Floquet, 2006), is housed
243 in two double-width 19 inch aircraft racks, with the inlet, detection cells, and pump set being
244 separate to the two racks. Ambient air is sampled through a 0.7 mm diameter ‘pinhole’ into a
245 cylindrical inlet (length = 50 cm, diameter = 5 cm) which extends through a window blank on
246 the starboard side of the aircraft.

247 Downstream of the inlet are two low pressure fluorescence cells positioned in series, the first
248 for detection of OH and the second for detection of HO₂. During the RONOCO and SeptEx
249 flights the pressure inside the cells ranged from 1.9 Torr at ground level to 1.2 Torr at 6 km.

250 Laser light at $\lambda \sim 308$ nm is generated by a diode-pumped Nd:YAG-pumped tunable
251 Ti:Sapphire laser (Photonics Industries DS-532-10 and TU-UV-308nm) and delivered to the
252 fluorescence cells via optical fibres, on an axis perpendicular to the gas flow. A small fraction
253 of the Ti:Sapphire second harmonic ($\lambda = 462$ nm) is directed to the probe of a wavemeter to
254 enable measurement of the laser wavelength to within 0.001 nm. A UV photodiode is
255 positioned opposite the laser input arm on each fluorescence cell to measure laser power.

256 The sampled air forms a supersonic gas expansion beam in which the rate of collision
257 between OH radicals and ambient air molecules is reduced. The OH fluorescence lifetime is
258 therefore extended to several hundred nanoseconds, significantly longer than the laser pulse,
259 so that the measured signal can be temporally discriminated from laser scattered light. OH is
260 excited from its ground state, $X^2\Pi_i(v'' = 0)$, to its first electronically excited state,
261 $A^2\Sigma^+(v' = 0)$, at $\lambda \sim 308$ nm. The resulting on-resonance fluorescence is detected by a UV-
262 sensitive channel photomultiplier tube on an axis perpendicular to both the gas flow and the
263 laser light. HO₂ is detected by titration with an excess of NO (Reaction (R7)), the resulting
264 OH being detected as described.

265 The FAGE instrument was calibrated prior to and following each field measurement period,
266 using a well-established method (Edwards et al., 2003; Faloona et al., 2004; Commane et al.,
267 2010). Light at $\lambda = 184.9$ nm from a mercury pen-ray lamp photolyses water vapour in a flow
268 of synthetic air inside an aluminium flow tube, generating OH and HO₂ at known
269 concentrations. The aircraft FAGE instrument's limit of detection (LOD) for OH and HO₂ is
270 determined by the instrument's sensitivity and the standard deviation of the background
271 signal. During the RONOCO and SeptEx fieldwork the 1σ LOD for a 5 minute averaging
272 period ranged between 0.64 and 1.8×10^6 molecule cm^{-3} for OH and between 5.9 and
273 6.9×10^5 molecule cm^{-3} for HO₂.

274 **3.2 RO₂-based interference in FAGE measurements of HO₂**

275 It has recently been shown that reaction of alkene-derived β -hydroxyalkyl peroxy radicals,
276 RO₂, with NO inside the HO₂ detection cell, can lead to interference in FAGE HO₂
277 measurements (Fuchs et al., 2011; Whalley et al., 2013). The magnitude of the interference
278 depends on the parent alkene, the residence time and mean temperature inside the cell, and
279 the amount of NO injected. The interference therefore depends on the chemical environment
280 and differs between FAGE instruments. In view of this, the University of Leeds ground-based

281 and aircraft FAGE instruments have been tested for RO₂ interference. A thorough description
282 of the ground-based experimental method and results, and the results of a modelling study,
283 are given by Whalley et al. (2013). The strongest interference in the aircraft instrument
284 measurements was observed for ethene-derived RO₂, amounting to an increase of 39.7 ± 4.8
285 % in the observed HO₂ signal, with a cell pressure of 1.8 Torr, an estimated detection cell
286 temperature of 255 K (obtained from rotational excitation spectra performed previously), and
287 [NO]_{cell} = 10¹⁴ molecule cm⁻³.

288 ~~Whalley et al. (2013) show that the chemistry responsible for the observed interferences is~~
289 ~~well known, and that a model using the Master Chemical Mechanism (MCM, version 3.2:~~
290 ~~Jenkin et al., 1997; Saunders et al., 2003; Bloss et al., 2005, via~~
291 ~~http://mcm.leeds.ac.uk/MCM) can reproduce the interferences once tuned to the conversion~~
292 ~~efficiency of HO₂ to OH in the FAGE detection cell. Accordingly,~~ Stone et al. (2014b) have
293 applied the results of the ethene-derived RO₂ interference testing in a modelling study to
294 assess the effect of the interference on the HO₂ measurements made during the RONOCO
295 and SeptEx campaigns. A box model using a detailed ~~MCMaster Chemical Mechanism~~
296 scheme was used to calculate a total potential interference in the RONOCO HO₂
297 measurements. The model was constrained to the conditions in the detection cell (1.8 Torr,
298 255 K, [NO] ~ 10¹⁴ molecule cm⁻³). Equal concentrations of HO₂ and ∑RO₂ (sum of all
299 peroxy radicals in the MCM generated from the parent hydrocarbon) were used to initialise
300 the model. The model ~~run time was varied until the model was predicted interference from~~
301 ~~ethene-derived RO₂ radicals was equal to the experimentally determined interference, thereby~~
302 ~~tuning the model to the conversion efficiency of HO₂ to OH, run until the modelled~~
303 ~~interference (i.e. concentration of OH produced) from ethene derived RO₂ radicals matched~~
304 ~~the interference measured in the interference experiments described above (~40%).~~ An
305 interference factor, *f*, was calculated for each RO₂ in the MCM as follows:

$$306 \quad f = \frac{[\text{OH}]_{\text{HO}_2+\text{RO}_2} - [\text{OH}]_{\text{HO}_2}}{[\text{OH}]_{\text{HO}_2}} \quad (1)$$

307 where [OH]_{HO₂+RO₂} and [OH]_{HO₂} are the modelled concentrations of OH produced from the
308 reactions of RO₂ and HO₂, and the concentration from HO₂ alone, respectively. The greatest
309 interference was calculated to come from isoprene-derived peroxy radicals, followed by
310 aromatic compounds and C₂ to C₅ alkenes. The smallest modelled interference is from the C₁
311 to C₃ alkanes. ~~The interference factors were applied to model-predicted RO₂ speciation and~~

Comment [HW3]: See Reviewers'
Comments Sect. 1.2

Comment [HW4]: See Reviewers'
Comments Sect 1.2, Sect. 2.2, and Sect 2.3

Comment [HW5]: See Reviewers'
Comments Sect 1.2

312 concentrations for the RONOCO flights. Model-predicted RO₂ species were dominated by
313 CH₃O₂ (33 %; *f* = 1.1 %) and HO₂ (24 %; *f* = 0.0 %), with smaller contributions from RO₂
314 derived from *iso*-butene (12 %; *f* = 0.5 %), *cis*-2-butene and *trans*-2-butene (10 %; *f* = 0.05
315 %), and isoprene (2 %; *f* = 7.6 %). RO₂ species with high interference factors were a minor
316 component of the total RO₂. A modelled value of HO₂ including the total potential
317 interference, [HO₂]*, was calculated using:

318
$$[\text{HO}_2^*] = [\text{HO}_2]_{\text{mod}} + f[\text{RO}_2]_{\text{mod}} \quad (2)$$

Comment [HW6]: Changed equation: “*” inside square brackets and not superscript

319 Direct comparison between modelled values of [HO₂*]^{*} and the FAGE-measured values of
320 [HO₂] was therefore made possible. The model-predicted interference during the RONOCO
321 campaign ~~is can be~~ described by [HO₂]^{*} = 1.15[HO₂] + 2 × 10⁵ molecule cm⁻³. The average
322 model-predicted interference in the HO₂ measurements is 14 %. The HO₂ measurements
323 made during RONOCO and SeptEx were not adjusted since speciated RO₂ measurements
324 were not available. The measurements are hereafter referred to as HO₂*.

Comment [HW7]: See Reviewers' Comments Sect. 2.4

Comment [HW8]: See Reviewers' Comments Sect. 1.1

325 The magnitude of the RO₂ interference can be reduced by reducing the concentration of NO
326 in the detection cell. This also reduces the instrument sensitivity to HO₂. Since conversion of
327 RO₂ to OH requires at least two NO molecules, while conversion of HO₂ requires only one
328 molecule, the ratio of HO₂ signal to RO₂ signal can be made favourable by reducing [NO]
329 (Whalley et al., 2013). This effect has been investigated for the ground-based instrument, and
330 will be investigated for the aircraft instrument prior to future HO_x measurement campaigns.
331 An overview of the laboratory and computational studies of the interference in different
332 FAGE instruments is given in a recent review by Stone et al. (2012).

333 **3.3 BBCEAS measurements of NO₃ and N₂O₅**

334 NO₃ and N₂O₅ were measured by the University of Cambridge broadband cavity enhanced
335 absorption spectroscopy (BBCEAS) instrument. The instrument was designed and built
336 specifically for the RONOCO project and is described in detail in Kennedy et al. (2011). A
337 brief description is given here.

338 The instrument consists of three 94 cm long high finesse optical cavities formed by pairs of
339 highly reflecting mirrors. The cavities are irradiated by incoherent broadband continuous
340 wave light sources. Two of the cavities, for the detection of N₂O₅ and NO₃, are irradiated by
341 red light emitting diodes (LEDs) centred at 660 nm. The third cavity, for the detection of
342 NO₂, is irradiated by a blue LED centred at 460 nm. The light from the LEDs is collimated

343 using optical fibres and a focussing lens at the input of each cavity. A spectrometer,
344 consisting of a spectrograph and charge couple device (CCD), is positioned at the end of each
345 cavity to measure the wavelength-dependent intensity of transmitted light.

346 Ambient air is sampled through a rear-facing inlet on the aircraft fuselage, positioned
347 approximately 4 m from the aircraft nose and 10 cm from the aircraft body. The air from the
348 inlet is divided into two flows. The flow directed to the N_2O_5 cavity is heated to 120 °C to
349 ensure near complete (> 99.6 %) thermal dissociation of N_2O_5 to NO_2 and NO_3 . The cavity
350 itself is heated to 80 °C and is used to measure the sum of the concentrations of ambient NO_3
351 plus NO_3 from thermal decomposition of N_2O_5 . The second flow is unheated and is directed
352 first through the NO_3 cavity and then through the NO_2 cavity. Background spectra are
353 recorded at half hour intervals during flights by halting the flow of ambient air and purging
354 the cavities with nitrogen.

355 NO_3 is detected by its strong $B^2E' - X^2A_2'$ electronic transition centred at 662 nm. The
356 concentration of NO_3 is determined by separating the finely structured NO_3 absorption
357 features from the broad features caused by Rayleigh and Mie scattering using a fitting
358 technique analogous to that employed in differential optical absorption spectroscopy
359 (DOAS). A strong water vapour absorption feature that spectrally overlaps with NO_3
360 absorption around 662 nm is simulated for the pressure and temperature measured in the
361 cavity and is removed from the measured absorption spectrum. The concentration of N_2O_5 is
362 determined by subtracting the concentration of ambient NO_3 measured in the unheated cavity
363 from the sum of the concentrations of ambient and dissociated NO_3 measured in the heated
364 cavity.

365 Contributions to uncertainties in ambient measurements of NO_3 and N_2O_5 , including wall
366 losses of NO_3 and N_2O_5 , temperature- and pressure-dependent absorption cross sections of
367 NO_3 and H_2O , and the length of the cavity occupied by the sample, have been thoroughly
368 investigated in laboratory experiments or addressed in the data analysis routine. In addition,
369 wall losses of NO_3 and N_2O_5 were determined before and after each flight to account for
370 changes in the surface properties of the inlet and detection cell walls, which were found to be
371 negligible. The total uncertainty in the measured concentration of ambient NO_3 was 11 %.
372 The uncertainty in the measured concentration of ambient N_2O_5 is determined for each
373 individual ambient measurement, being dependent on the NO_3/N_2O_5 ratio, and was on the

Comment [HW9]: See Reviewers'
Comments Sect 2.5

374 order of 15 %. During RONOCO flights the 1σ limits of detection for NO_3 and the sum of
375 $\text{NO}_3 + \text{N}_2\text{O}_5$ were 1.1 pptv and 2.4 pptv, respectively, for a 1 second integration time.

376

377 **4 Overview of OH and HO₂* measurements**

378 FAGE measurements were made on 16 flights during RONOCO and 9 flights during SeptEx.

379 There was insufficient laser power during flights B534 to B536 in the summer campaign to
380 measure both OH and HO₂* by dividing the laser light between the two cells. OH was
381 therefore not measured during these flights. Low laser power throughout the summer
382 fieldwork caused relatively high fluctuations in laser power and therefore higher background
383 variability. This resulted in higher limits of detection for OH (1.8×10^6 molecule cm^{-3}) and
384 HO₂* (6.9×10^5 molecule cm^{-3}).

385 Table 4 summarises the OH and HO₂* measurements during RONOCO and SeptEx and gives
386 the instrument's average 1σ limit of detection for ~~a 5one~~ minute ~~averaging period of data~~. OH
387 was not detected above the limit of detection during the summer or winter RONOCO flights,
388 resulting in upper limits of 1.8×10^6 molecule cm^{-3} and 6.4×10^5 molecule cm^{-3} for mean
389 summer and winter concentrations, respectively. These upper limit values are similar to
390 previously reported nighttime OH measurements (Geyer et al., 2003; Holland et al., 2003;
391 Ren et al., 2003b; Emmerson and Carslaw, 2009). The mean daytime OH concentration
392 during SeptEx was 1.8×10^6 molecule cm^{-3} , which was above the limit of detection. The
393 mean HO₂* mixing ratio was highest during SeptEx (2.9 pptv), and was higher during
394 summer (1.6 pptv) than during winter (0.7 pptv). The OH and HO₂* datasets for RONOCO
395 and SeptEx are shown as altitude profiles in Fig. 43 and Fig. 54, respectively.

396 Table 5 gives the mean and maximum HO₂* mixing ratios at different times of day during
397 summer, SeptEx and winter. Dawn, day, dusk and night are defined by the solar zenith angle
398 as follows: dawn and dusk are between 90 and 102° and are distinguished by the time of day;
399 day is between 0° and 90° ; night is between 102° and 180° .

400 The mean dusk HO₂* mixing ratio in summer was higher than the mean nighttime mixing
401 ratio, suggesting that photochemical production was still active at dusk in summer. The
402 reverse was true for the winter data, with the highest mean HO₂* mixing ratio being at night.
403 This suggests that when photochemical production was suppressed in the winter daytime due
404 to low photolysis rates, production via reactions of NO_3 and O_3 with alkenes was an
405 important route to radical initiation. The RONOCO HO₂* measurements are similar to

Comment [HW10]: See Reviewers'
Comments Sect 1.3

406 nighttime, ground-based, urban measurements. For example, during the TORCH campaign,
407 [HO₂] peaked at 1×10^8 molecule cm⁻³ at night (Emmerson et al., 2007), and during the
408 PMTACS-NY 2001 field campaign, nighttime HO₂ concentrations of 8×10^6 molecule cm⁻³
409 were measured (Ren et al., 2003b).

410 **4.1 Case study flight B537: high nighttime HO₂* concentrations**

411 The highest HO₂* concentration (3.2×10^7 molecule cm⁻³; 13.7 pptv) was measured during
412 nighttime flight B537 on 20th July 2010. Take-off from East Midlands Airport was at 22:00
413 local time (21:00 UTC, sunset at 20:18 UTC). The flight track, coloured by altitude, is shown
414 in Fig. 65. The flight involved a profile descent from 3350 m to 460 m down the Norfolk
415 coast and a missed approach at Southend Airport (51.6° N, 0.70° E). Plumes from European
416 continental outflow (see Fig. 76) were intersected by a series of runs at altitudes between 460
417 m and the upper boundary of the polluted layer.

418 Flight B537 is an unusual flight within the RONOCO dataset, with high concentrations of
419 CO, O₃, NO₃, and high temperatures compared to the values measured during other nighttime
420 flights (see Table 3). The ambient aerosol surface area was significantly higher during B537
421 (nearly 800 μm² cm⁻³) than during other flights (between 100 and 400 μm² cm⁻³), and the
422 organic aerosol concentration was significantly enhanced (Morgan et al., 2014). Footprint
423 maps for flight B537, indicating regions where the sampled air was in contact with the
424 surface prior to the flight, are shown in Fig. 67. The air sampled during the flight originated
425 primarily over northern France, Belgium and Germany.

426 A region of high surface pressure was positioned over the UK on the 20th July, with a mean
427 air pressure of 1012.6 hPa over the 24 hours prior to the flight. The mean air temperature 24
428 hours prior to the flight (22:00 19/07/2010 to 22:00 20/07/2010), measured at a number of
429 Met Office weather stations in Greater London, was 22.6 °C, and reached a maximum value
430 of 28.6 °C. Wind speeds prior to the flight were low, with an average value of 4.7 knots
431 (2.4 m s⁻¹). No rainfall was recorded at any of the Greater London weather stations during the
432 24 hours prior to the flight. 12.4 hours of sunshine were recorded on the 20th July at
433 Heathrow Airport (51.5 °N, 0.45 °W). High temperatures, combined with low wind speed,
434 exposure to solar radiation, and little precipitation promote the formation of ozone as a result
435 of photochemical processing of VOCs emitted at the surface (e.g. Lee et al., 2006), and offer
436 an explanation for the high ozone mixing ratios measured during flight B537. Peak surface
437 daytime ozone concentrations measured in Teddington, London, on 20th July were on the

438 order of 2.0×10^{12} molecule cm^{-3} (~78 ppbv) (data available at www.airquality.co.uk).
439 Similar levels were recorded at a number of locations within Greater London.

440 ~~Figure 8~~Figure 7 shows a time series of altitude, HO₂^{*}, O₃, and NO₃ mixing ratios during the
441 flight, demonstrating very similar behaviour between the two radical species. During the
442 missed approach at Southend Airport the mixing ratios of HO₂^{*} and NO₃ increased with
443 decreasing altitude, to reach values of 4.5 pptv and 35 pptv, respectively, at 50 m above the
444 ground. The maximum HO₂^{*} and NO₃ mixing ratios were measured over the North Sea east
445 of Ipswich (52.16 ° N, 2.34 ° E) at an altitude of 509 m, in the outflow of the London plume.
446 ~~Figure 9~~Figure 8 shows scatter plots of HO₂^{*} against NO₃ and O₃ during flight B537 and
447 during the other nighttime flights during RONOCO. Strong positive correlation is evident
448 between HO₂^{*} and NO₃ during B537 ($r = 0.97$), while during the remaining night flights
449 there is still a significant, though weaker, correlation ($r = 0.58$). Moderate negative
450 correlation is evident between HO₂^{*} and O₃ during B537 ($r = -0.46$), with weak positive
451 correlation existing for the other nighttime flights ($r = 0.19$). The data suggest that NO₃ was
452 an important initiator of HO_x radicals during flight B537, and that O₃ played a limited role
453 overall during the nighttime flights. Further investigation of the roles of NO₃ and O₃ in alkene
454 oxidation and radical initiation at night is described in Sect. 5.

455

456 5 Oxidation of alkenes and production of HO₂: method of analysis

457 Following the work of Salisbury et al. (2001), the total rates of reaction, Φ , of O₃ and NO₃
458 with the alkenes measured during RONOCO and SeptEx have been calculated:

$$459 \quad \Phi_{\text{O}_3} = \sum_i^{\text{alkene}} k_{\text{O}_3+\text{alk}_i} [\text{O}_3][\text{alkene}_i] \quad (3)$$

$$460 \quad \Phi_{\text{NO}_3} = \sum_i^{\text{alkene}} k_{\text{NO}_3+\text{alk}_i} [\text{NO}_3][\text{alkene}_i] \quad (4)$$

461 The reactions of O₃ and NO₃ with alkenes yield OH, HO₂, and RO₂ radicals. Consideration of
462 the reaction mechanisms of NO₃ and O₃ enables calculation of the rate of instantaneous
463 production of HO₂ (P_{HO_2}) from the reactions of NO₃ and O₃ with the alkenes measured
464 during RONOCO, using the chemistry scheme, rate constants and branching ratios in the
465 MCM (Jenkin et al., 1997; Saunders et al., 2003).

466 ~~Figure 10~~Figure 9 shows a generalized reaction scheme for the reaction of NO₃ with an
 467 alkene. The reaction between NO₃ and an alkene proceeds via addition of NO₃ to the double
 468 bond to form a nitrooxyalkyl radical, followed by rapid reaction with oxygen to yield a
 469 nitrooxyalkyl peroxy radical, RO₂ (shown as a single step in Fig. 109). The RO₂ radical can
 470 react with a number of species, of which NO, NO₃ and RO₂ lead to production of an alkoxy
 471 radical (RO). Radical termination occurs via reaction of RO₂ with HO₂ to yield a peroxide
 472 (ROOH) or with RO₂ to yield carbonyl (RC(O)CH₃) and alcohol (RCH₂OH) products.
 473 Reaction of RO with oxygen proceeds via abstraction of a hydrogen atom to yield HO₂ or an
 474 aldehyde (RCHO). This generalised scheme can be applied to the reactions of NO₃ with all
 475 the alkenes measured. The rate of instantaneous production of HO₂ is found by first
 476 calculating the fraction of RO₂ that reacts to produce RO (F_{RO}), and the fraction of RO that
 477 reacts to produce HO₂ (F_{HO_2}):

$$478 \quad F_{RO} = \frac{k_3[NO] + k_4[NO_3] + 0.6k_5[RO_2]}{k_2[HO_2] + k_3[NO] + k_4[NO_3] + k_5[RO_2]} \quad (5)$$

$$479 \quad F_{HO_2} = \frac{k_6[O_2]}{k_7 + k_6[O_2]} \quad (6)$$

480 where RO₂ represents all peroxy radicals. Average values of F_{RO} for the NO₃ + alkene
 481 reactions range between 0.50 for *trans*-2-pentene- and 1-pentene-derived RO₂ species and
 482 0.61 for ethene-derived RO₂ species. F_{HO_2} varies between 0 and 1 for the alkenes studied.

483 Overall, the rate of production of HO₂ (P_{HO_2}) from reactions of NO₃ with alkenes is then
 484 given by:

$$485 \quad P_{HO_2} = k_i[NO_3][\text{alkene}_i] \times F_{RO} \times F_{HO_2} \quad (7)$$

486 The reaction scheme for the reaction of O₃ with alkenes is more complicated because the
 487 number and type of radicals produced in the O₃ + alkene reaction depends on the structure of
 488 the alkene. The simplest case is the reaction of ozone with ethene. Ozone adds to the double
 489 bond to form a five-membered ring called a primary ozonide. Decomposition of the ozonide
 490 yields an excited Criegee intermediate (CH₂OO*) and a carbonyl compound (in this case
 491 formaldehyde, HCHO). The energy-rich Criegee intermediate can be stabilised by collision
 492 with a third body or undergo decomposition to yield products including OH, CO, and HO₂.
 493 The primary ozonide produced in the O₃ + propene reaction (see Fig. 110) can decompose via
 494 two channels, yielding carbonyls and Criegee intermediates with different structures and

Comment [HW11]: See Reviewers'
 Comments Sect 2.6

Field Code Changed

495 different products, including RO₂. Reaction of RO₂ with NO, NO₃ and RO₂ (all peroxy
496 radicals) yields RO, which in turn yields HO₂.

497 The rates of production of HO₂ from reactions of O₃ with alkenes (P_{HO_2}) have been
498 calculated as follows:

$$499 \quad P_{\text{HO}_2, \text{Direct}} = k_i [\text{O}_3] [\text{alkene}_i] \times \alpha_{\text{HO}_2} \quad (8)$$

$$500 \quad P_{\text{HO}_2, \text{RO}_2} = k_i [\text{O}_3] [\text{alkene}_i] \times \alpha_{\text{RO}_2} \times F_{\text{RO}} \times F_{\text{HO}_2} \quad (9)$$

$$501 \quad P_{\text{HO}_2} = P_{\text{HO}_2, \text{Direct}} + P_{\text{HO}_2, \text{RO}_2} \quad (10)$$

502 where $P_{\text{HO}_2, \text{Direct}}$ is the rate of direct HO₂ production from Criegee intermediate
503 decomposition, α_{HO_2} is the branching ratio to HO₂-producing channels from the Criegee
504 intermediate, $P_{\text{HO}_2, \text{RO}_2}$ is the rate of HO₂ production from RO₂ radicals produced in the O₃ +
505 alkene reaction, α_{RO_2} is the branching ratio to RO₂-producing channels from the Criegee
506 intermediate, F_{RO} is the fraction of RO₂ radicals that react to produce RO radicals, and F_{HO_2}
507 is the fraction of RO radicals that react to produce HO₂ radicals, which is equal to 1 for all the
508 alkenes studied. Average values of F_{RO} for the O₃ + alkene reactions range between 0.54 for
509 1-pentene-derived RO₂ species and 0.64 for 1-butene- and *trans*-2-pentene-derived RO₂
510 species.

Comment [HW12]: See Reviewers'
Comments Sect. 2.6

Field Code Changed

511 The reactions of RO₂ with NO to form RONO₂ have been omitted from the calculations
512 because the branching ratio is small (0.001 to 0.02) for the radicals studied (Carter and
513 Atkinson, 1989; Lightfoot et al., 1992). The reaction of CH₃O₂ with NO₂ to form CH₃O₂NO₂
514 has been omitted from the calculations, since the reverse reaction is much faster than the
515 forward direction ($k_f = 6.4 \times 10^{-12} \text{ s}^{-1}$; $k_{\text{rev}} = 1.08 \text{ s}^{-1}$ at a mean temperature of 286.5 K during
516 RONOCO).

517 The primary aims of the analysis presented here are threefold: 1. To calculate the total rate of
518 initiation through reactions of NO₃ and O₃ with alkenes; 2. To determine the relative
519 importance of NO₃ and O₃ in nighttime HO₂ production; 3. To investigate differences in
520 radical production between different seasons and different times of day. The correlation
521 between [HO₂*] and [NO₃], especially during flight B537, will be investigated.

522 P_{HO_2} has been calculated for each alkene measured for every 60-second data point where all
523 the requisite data were available and where HO₂* was above the limit of detection of the

524 FAGE instrument. Concentrations of RO₂ were calculated by scaling the observed HO₂*
525 concentrations with the RO₂/HO₂* ratio calculated using a box model constrained to the
526 concentrations of long-lived species measured during the flights (Stone et al., 2014b), i.e.
527 $RO_{2,obs} = HO_{2,obs}^* \times RO_{2,mod}/HO_{2,mod}^*$. The rates of reaction and rates of production of HO₂
528 presented hereafter are average values for individual flights, seasons, or times of day.

Comment [HW13]: See Reviewers'
Comments Sect. 1.4

530 6 Results

531 6.1 Nighttime oxidation of alkenes

532 ~~Figure 12~~Figure 11 shows histograms of the rate of reaction between O₃ and NO₃ with
533 individual alkenes during summer and winter, for the nighttime data only. The reactivity of
534 measured alkenes ($\Phi_{O_3} + \Phi_{NO_3}$) was greater during summer flights than during winter flights
535 by a factor of 2.2. The reactions of NO₃ are largely responsible for this seasonal difference,
536 since the contribution from O₃ + alkene reactions varies little between summer
537 (4.1×10^4 molecule cm⁻³ s⁻¹) and winter (3.9×10^4 molecule cm⁻³ s⁻¹). The factor of 4.1
538 difference between the rate of NO₃ reactions in summer (9.8×10^4 molecule cm⁻³ s⁻¹) and
539 winter (2.4×10^4 molecule cm⁻³ s⁻¹) can be attributed to the higher mean concentration of
540 NO₃ in summer (5.8×10^8 molecule cm⁻³) compared to winter (2.0×10^8 molecule cm⁻³).

541 This seasonal difference in NO₃ concentrations ~~is attributable to~~ may have been the result of
542 the lower mean nighttime temperature in winter (277.7 K) compared to summer (286.7 K)
543 which disfavours NO₃ in ~~the its~~ thermal equilibrium ~~with~~ $N_2O_5 \rightleftharpoons NO_3 + NO_2$. $K_{eq}[NO_2]$,
544 which determines $[N_2O_5]/[NO_3]$, is calculated to be 4.8 in summer and 29.6 in winter. At

Comment [HW14]: See Reviewers'
Comments Sect. 2.7

545 night in summer, Φ_{NO_3} was greater than Φ_{O_3} by a factor of 2.4, but in winter Φ_{O_3} was a factor
546 of 1.6 greater than Φ_{NO_3} . ~~Figure 12~~Figure 11 illustrates the importance of the butene isomers
547 (within the VOCs measured) in the reactions of O₃ and NO₃, and therefore radical initiation
548 and propagation. Reactions with *iso*-butene dominated NO₃ reactivity in summer (42 %) and
549 winter (53 %), with *trans*-2-butene also contributing significantly (28 % in summer and 32 %
550 in winter). Reactions of O₃ were dominated by *trans*-2-butene (42 % in summer and 34 % in
551 winter) and propene (26 % in summer and 38 % in winter). The importance of these alkenes
552 is attributed to their relatively high abundances compared to the other alkenes measured,
553 during both summer and winter, combined with their fast rates of reaction with O₃ and NO₃.

Comment [HW15]: See Reviewers'
Comments Sect. 2.7

554 For comparison with the reactions of O₃ and NO₃, the total rate of reaction of measured
555 alkenes with OH has been calculated using upper limits on OH concentrations of 1.8×10^6

556 molecule cm^{-3} and 6.4×10^5 molecule cm^{-3} for the summer and winter flights, respectively,
557 based on the FAGE instrument's limit of detection. The high upper limits make the total rate
558 of reaction of OH with alkenes, Φ_{OH} , unrealistically high for both summer (1.6×10^5
559 molecule $\text{cm}^{-3} \text{ s}^{-1}$) and winter (7.8×10^4 molecule $\text{cm}^{-3} \text{ s}^{-1}$). However, the OH reactivity will
560 likely be considerably lower than the values calculated using the OH upper limits. A box
561 model constrained to concentrations of long-lived species measured during the flights (Stone
562 et al., 2014b) predicts a mean OH concentration of 2.4×10^4 molecule cm^{-3} , significantly
563 lower than the upper limits given by the instrument's limit of detection. Using the mean
564 modelled value for OH gives $\Phi_{\text{OH}} = 2.1 \times 10^3$ molecule $\text{cm}^{-3} \text{ s}^{-1}$ for summer, and $\Phi_{\text{OH}} =$
565 2.9×10^3 molecule $\text{cm}^{-3} \text{ s}^{-1}$ for winter, indicating a diminished role for OH in alkene
566 oxidation at night in agreement with previous studies (e.g. Geyer et al., 2003; Emmerson et
567 al., 2005).

568 **6.2 Daytime oxidation of alkenes**

569 **Figure 13** ~~Figure 12~~ shows histograms of rates of reaction of O_3 and OH with alkenes during
570 SeptEx, and O_3 and NO_3 with alkenes during winter RONOCO flights, for daytime data only.
571 OH was detected above the limit of detection (1.2×10^6 molecule cm^{-3}) during the SeptEx
572 flights, so the FAGE OH data were included in the calculations, using a reaction scheme
573 analogous to the one shown in Fig. 109. NO_3 was not detected during the day in SeptEx. NO_3
574 is not expected to be present at measurable concentrations during daylight hours due to
575 photolysis, but a mean concentration of 8.3×10^7 molecule cm^{-3} (3.3 pptv) was measured
576 during the day in the winter RONOCO flights. These measurements of low mixing ratios of
577 NO_3 may be partly caused by interference from other daytime species as observed by Brown
578 et al. (2005), or by the variability of the instrument baseline, which can be on the order of 1–2
579 pptv during vertical profiles on the aircraft (Kennedy et al., 2011). This variability is small
580 compared to the range of NO_3 values typically observed during RONOCO flights (0–50 pptv
581 during summer; 0–10 pptv during winter). During SeptEx, Φ_{OH} exceeded Φ_{O_3} by a factor of
582 8. Ethene and propene were the two most abundant alkenes measured during SeptEx and
583 contributed significantly to OH reactivity. O_3 reactivity with alkenes was dominated by
584 propene and *trans*-2-butene (6th most abundant alkene measured during SeptEx). NO_3
585 reactivity with alkenes was dominated by *trans*-2-butene and isobutene (3rd most abundant
586 alkene measured during winter daytime flights). The total rate of reaction of O_3 and OH with
587 alkenes during daytime SeptEx flights (3.7×10^5 molecule $\text{cm}^{-3} \text{ s}^{-1}$) exceeded the total rate of

588 reaction of O₃ and NO₃ during daytime winter RONOCO flights (6.6×10^4 molecule cm⁻³
589 s⁻¹) by a factor of 6, and was more than double the total rate of reaction of O₃ and NO₃ with
590 alkenes during nighttime summer flights (1.4×10^5 molecule cm⁻³ s⁻¹). In winter daytime
591 flights, Φ_{O_3} was greater than Φ_{NO_3} by a factor of 2.4.

592 ~~Figure 11b~~ and Fig. 132b reveal that reactions of O₃ dominated alkene reactivity
593 during both daytime and nighttime winter RONOCO flights. The concentrations of alkenes
594 were generally higher at night, with the total alkene concentration (sum of concentrations of
595 alkenes measured) being 2.1×10^9 molecule cm⁻³ in the day, and 3.4×10^9 molecule cm⁻³ at
596 night. The total measured alkene reactivity ($\Phi_{O_3} + \Phi_{NO_3}$) was marginally higher during the
597 day, by a factor of 1.04. This difference is attributable mainly to the change in Φ_{O_3} .

598 Comparison of Fig. 124a and Fig. 132b reveals that the total measured alkene reactivity
599 ($\Phi_{O_3} + \Phi_{NO_3}$) was higher during the summer nighttime flights (1.4×10^5 molecule cm⁻³ s⁻¹)
600 than during the winter daytime flights (6.6×10^4 molecule cm⁻³ s⁻¹), indicating a low
601 oxidising environment during winter daytime. The additional contribution to measured alkene
602 reactivity from reactions with OH has been calculated using the OH upper limits as described
603 in Sect. 6.1. Even with this additional, upper limit OH reactivity (1.6×10^5 molecule cm⁻³ s⁻¹
604 and 1.1×10^5 molecule cm⁻³ s⁻¹ for summer nighttime and winter daytime, respectively) the
605 total summer nighttime alkene reactivity remains higher than that during winter daytime,
606 confirming the importance of the summer nocturnal troposphere for the oxidation of the
607 measured alkenes.

608 **6.3 Nighttime production of HO₂ from reactions of O₃ and NO₃ with alkenes**

609 Table 6 gives total rates (ΣP_{HO_2}) of instantaneous production of HO₂ from the reactions of O₃
610 and NO₃ with alkenes. NO₃ was not detected during the dawn summer RONOCO flights and
611 there were no daytime RONOCO flights during summer. NO₃ dominated HO₂ production
612 during dusk and night (68 %), in agreement with Geyer et al. (2003) who found that NO₃ was
613 responsible for 53 % of HO₂ production at night in the BERLIOZ campaign. During winter,
614 O₃ dominated HO₂ production at all times, with a nighttime contribution of 70 %. This is in
615 agreement with the results from the winter PMTACS-NY 2004 field campaign (Ren et al.,
616 2006).

617 The total rate of instantaneous production of HO₂ at night was 3.3 times greater in summer
618 than in winter, with production from O₃ decreasing by a factor of 1.5, and production from
619 NO₃ decreasing by a factor of 7.8, between summer and winter. The mean temperature

620 difference between summer and winter of 9 K is thought to be responsible for the lower NO₃
621 concentrations in winter (2.0×10^8 molecule cm⁻³, 8.2 pptv, compared to 5.8×10^8 molecule
622 cm⁻³, 24.5 pptv in summer), owing to the increased thermal stability of N₂O₅, and for the
623 reduced rate of temperature-dependent reactions between NO₃ and alkenes, and subsequent
624 reactions. There was very little difference between summer and winter mean O₃ mixing
625 concentrations (9.6×10^{11} molecule cm⁻³, 39.6 ppbv, and 9.4×10^{11} molecule cm⁻³, 38.6
626 ppbv, respectively).

627 Production of HO₂ via reactions of NO₃ and O₃ with alkenes is now examined in more detail.
628 The rate of production from individual alkenes was calculated, and plotted in a histogram, as
629 shown in Fig. 143 for the summer and winter nighttime data. During both summer and
630 winter, reactions of O₃ and NO₃ with *trans*-2-butene were important sources of HO₂,
631 contributing on average 62 % to O₃-initiated HO₂ production and 36 % to NO₃-initiated
632 production during the summer and winter flights. Reactions of NO₃ with isoprene were
633 important during summer, contributing 28 % to NO₃-initiated production. The importance of
634 *trans*-2-butene, despite its relatively low abundance during summer and winter nighttime
635 RONOCO flights (1.8 pptv and 1.7 pptv, respectively, compared to ethene mixing ratios of
636 55.0 and 104.5 pptv), is attributed to its fast rates of reaction with both O₃ and NO₃ compared
637 to the other alkenes measured. The importance of the isoprene + NO₃ reactions during the
638 summer RONOCO flights is similarly attributed to its fast rate of reaction with NO₃
639 compared to the other alkenes measured. In addition there is no aldehyde-forming channel
640 from the isoprene-derived RO radical (k_7 in Fig. 109), so that the yield of HO₂ from RO is
641 equal to 1. The reaction of isobutene with NO₃ can proceed via one of two channels to
642 produce two different RO₂ radicals but only one channel, with a branching ratio of 0.2,
643 produces HO₂. Isobutene is therefore not a dominant contributor to HO₂ production, despite
644 being the single largest contributor to NO₃ reactivity during daytime and nighttime RONOCO
645 flights (Fig. 124 and Fig. 132). ~~Figure 14~~Figure-13 highlights the small change in total
646 production from O₃ between summer and winter, and the dramatic change in total production
647 from NO₃ between summer and winter.

648 Reactions of formaldehyde with NO₃ were included in the analysis where formaldehyde data
649 were available (mean HCHO = 955 pptv). The NO₃ + HCHO reaction contributed a further
650 5.5×10^3 molecule cm⁻³ s⁻¹ (15 %) to HO₂ production from NO₃ reactions, so that production
651 from NO₃ contributed 79 % of the total production.

652 **6.4 Production of HO₂ during flight B537**

653 Flight B537, on 20th July 2010, has been identified as an interesting flight, with high
654 concentrations of HO₂* (3.2 × 10⁸ molecule cm⁻³; 13.6 pptv), ozone (peaking at
655 1.8 × 10¹² molecule cm⁻³, 89.9 ppbv) and NO₃ (peaking at 4.1 × 10⁹ molecule cm⁻³;
656 176.9 pptv), and a strong positive correlation between HO₂* and NO₃ ($r = 0.97$, see Fig. 98).
657 NO, NO₂, and aerosol surface area were also elevated during the flight during flight B537
658 compared to their mean summer values. The highest concentration of ethene (1.43 × 10¹⁰
659 molecule cm⁻³; 0.61 ppbv) during the summer RONOCO flights was measured during B537.
660 ΣP_{HO_2} from O₃ + alkene reactions (2.6 × 10⁴ molecule cm⁻³ s⁻¹) was higher in flight B537
661 than in all the other summer flights, contributing 42 % of HO₂ production, with NO₃ + alkene
662 reactions contributing 3.6 × 10⁴ molecule cm⁻³ (58 %). The total rate of HO₂ production from
663 O₃ and NO₃ reactions during flight B537 was 6.2 × 10⁴ molecule cm⁻³ s⁻¹. While this is
664 higher than the average value of ΣP_{HO_2} for the summer flights (5.4 × 10⁴ molecule cm⁻³ s⁻¹) it
665 is not the highest rate of production during the summer flights. During B534 unusually high
666 concentrations of isoprene, *cis*-2-butene, and 1,3-butadiene contributed to a total rate of HO₂
667 production of 7.9 × 10⁴ molecule cm⁻³, which is the highest calculated value.

668 [Figure 15](#)~~Figure 14~~ shows that the reactions of O₃ and NO₃ with *trans*-2-butene are once
669 again important, contributing 74 % of $\Sigma P_{\text{HO}_2, \text{O}_3}$, and 45 % of $\Sigma P_{\text{HO}_2, \text{NO}_3}$. The correlation
670 between HO₂* and NO₃ is attributed to production of HO₂ by reactions of NO₃ with alkenes,
671 especially *trans*-2-butene. Figure 165 shows HO₂* versus the total instantaneous rate of
672 production from the reactions of O₃ and NO₃ with alkenes during flight B537, at each 60-
673 second data point during the flight for which the requisite data were available. Note that the
674 rates plotted in Fig. 165 are higher than those shown in Fig. 154, where the rates of
675 production of HO₂ from each alkene have been averaged across the whole flight. A strong
676 positive correlation exists between HO₂* and both $\Sigma P_{\text{HO}_2, \text{O}_3}$ ($r = 0.6$) and $\Sigma P_{\text{HO}_2, \text{NO}_3}$ ($r = 0.8$),
677 indicating the importance of these reactions for production of HO₂ during this flight.

678

679 **7 Comparison with model results**

680 The observations of OH, HO₂*, NO₃ and N₂O₅ have been interpreted in the context of
681 nighttime oxidation chemistry using a box model constrained to observations of VOCs, NO_x,
682 O₃, CO and other long-lived species measured during the RONOCO flights (Stone et al.,
683 2014b). The Dynamically Simple Model of Atmospheric Chemical Complexity (DSMACC)

684 (Emmerson and Evans, 2009; Stone et al., 2010; Stone et al., 2014b) was initiated with
685 concentrations of measured species, using a chemistry scheme based on the Master Chemical
686 Mechanism (MCM, version 3.2: Jenkin et al., 1997; Jenkin et al., 2003; Saunders et al., 2003;
687 Bloss et al., 2005, via <http://mcm.leeds.ac.uk/MCM>) and was allowed to run to diurnal steady
688 state. The model output includes concentrations of OH, HO₂, NO₃, RO₂, and other species.
689 Data from daytime flights, or during dawn or dusk periods, were not included in the model
690 analysis. Data from flight B537 were also excluded, owing to the atypical observations of
691 HO₂^{*}, NO₃, O₃ and other chemical species made during this flight. The modelling study and
692 results are described in more detail by Stone et al. (2014b).

693 The model predicts a mean OH concentration of 2.4×10^4 molecule cm⁻³ for the summer
694 flights, which is consistent with the measured OH concentrations for which the instrument's
695 limit of detection is an upper limit only. The base model underpredicts HO₂^{*} by around
696 200 %, and overpredicts NO₃ and N₂O₅ by 80 and 50 %, respectively. These discrepancies
697 were investigated by determining the processes controlling radical production and loss in the
698 model, and using those results to improve model performance. Model production of HO₂ is
699 dominated by reactions of RO + O₂ (42 %), with a significant contribution from OH + CO
700 (31 %) despite low OH concentrations at night. RO_x (= RO + RO₂ + OH + HO₂) radical
701 initiation in the model is dominated by reactions of NO₃ with unsaturated VOCs (80 %), with
702 a much smaller contribution (18 %) from alkene ozonolysis. Modelled HO₂ loss is dominated
703 by its reactions with NO₃ (45 %) and O₃ (27 %), both of which are radical propagating routes,
704 and which are the dominant routes to OH production in the model. In fact NO₃ was found to
705 control both radical initiation and propagation in the model.

706 These results are in general agreement with the results of the analysis presented in Sect. 6.1,
707 though the model predicts a more important role for NO₃ (80 % of RO_x radical production,
708 which is 7.2 times the contribution from O₃ + alkenes) than is predicted by the analysis based
709 on the observations alone (69 % of HO₂ radical production during summer, which is 2.1
710 times the contribution from O₃ + alkenes). ~~The model, and~~ predicts a relatively small role for
711 O₃ ~~in in both summer and winter radical initiation (18 % of RO_x radical production compared~~
712 ~~to a minimum value of 31 % calculated using the observations)~~. The model is constrained to
713 measured values of O₃, but overpredicts NO₃. The mean measured NO₃ nighttime mixing
714 ratio was 24.5 pptv in the summer and 8.2 pptv in the winter. The mean modelled summer
715 and winter values are 37.4 pptv and 20.7 pptv, respectively. This discrepancy between
716 modelled and measured NO₃ helps to explain the model overprediction of the role of NO₃ in

Formatted: Not Superscript/ Subscript

Comment [HW16]: See Reviewers' Comments Sect. 2.8

717 HO_x radical initiation during the RONOCO flights. Modelled NO₃ reactivity was dominated
718 by *iso*-butene (36 %) and *trans*-2-butene (27 %), and modelled O₃ reactivity was dominated
719 by *trans*-2-butene (51 %), in agreement with the nighttime alkene reactivities presented in
720 Sect. 6.1.

721 Improvement to the model predictions of NO₃, N₂O₅ and HO₂* was made by increasing the
722 concentration of unsaturated VOCs in the model. Increasing the total observed alkene
723 concentration by 4 times resulted in a modelled to observed ratio of 1.0 for HO₂* and of ~1.2
724 for NO₃ and N₂O₅. Two-dimensional gas chromatography (GC × GC) analysis of the whole
725 air samples taken during RONOCO has revealed a large number of VOCs extra to those
726 routinely measured (Lidster et al., 2014). Calibration standards for the majority of these
727 species are not yet available, and so quantification of their concentrations is not possible, but
728 their detection confirms that the model overprediction of NO₃ and underprediction of HO₂*
729 are attributable to reactions of NO₃ with unquantified unsaturated hydrocarbons.

730 The presence of unquantified unsaturated VOCs during the RONOCO campaign, suggested
731 by the model and confirmed by the two-dimensional GC analysis, has implications for the
732 conclusions drawn from the analysis based on the observations. The relative contributions of
733 NO₃ and O₃ to nighttime radical initiation will change with the composition of unsaturated
734 VOCs in the sampled air, due to the different rates of reaction of NO₃ and O₃ with different
735 VOC species, and the rates of production of HO₂ following these reactions. The model results
736 indicate that reaction of NO₃ with the unquantified VOCs leads to increased production of
737 HO₂. The role of NO₃ in nighttime radical production would therefore be enhanced by the
738 inclusion of the unquantified VOCs in the observational analysis.

739

740 **8 Conclusions and future work**

741 Nighttime radical chemistry has been studied as part of the RONOCO and SeptEx campaigns
742 onboard the BAe-146 research aircraft during summer 2010 and winter 2011. NO₃, N₂O₅, OH
743 and HO₂* were measured simultaneously for the first time from an aircraft, with OH and
744 HO₂* being measured by the University of Leeds aircraft FAGE instrument. OH was detected
745 above the limit of detection during the daytime SeptEx flights only, with a mean
746 concentration of 1.8×10^6 molecule cm⁻³. Upper limits of 1.8×10^6 molecule cm⁻³ and
747 6.4×10^5 molecule cm⁻³ are placed on mean OH concentrations for the summer and winter
748 RONOCO (night, dawn, and dusk) measurement campaigns, respectively. HO₂* was detected

Formatted: Not Superscript/ Subscript

Formatted: Not Superscript/ Subscript

Formatted: Not Superscript/ Subscript

749 above the limit of detection during the summer and winter RONOCO flights and during
750 SeptEx, with a maximum mixing ratio of 13.6 pptv measured during nighttime flight B537 on
751 20th July 2010. Mean nighttime HO₂* mixing ratios were significantly higher in summer than
752 in winter. Significant concentrations (up to 176.9 pptv) of NO₃ were measured during
753 nighttime flights, since the air masses sampled were sufficiently removed from the surface
754 that the loss of NO₃ by reaction with NO was minimised. The RONOCO flights were
755 therefore an excellent opportunity to study the role of NO₃ in nocturnal oxidation and radical
756 initiation.

757 The rates of reaction of O₃ and NO₃ with the alkenes measured have been calculated. At night
758 during summer, NO₃ dominated alkene reactivity. Several previous nighttime studies have
759 also found NO₃ to be the dominant nocturnal oxidant (e.g. Geyer et al., 2003; Brown et al.,
760 2011). During nighttime winter RONOCO flights the total rate of reaction of NO₃ with
761 alkenes was much reduced, but the rate of reaction of O₃ with alkenes was similar to that in
762 summer. During day and night in winter, O₃ + alkene reactions were faster than NO₃ + alkene
763 reactions. Overall, during RONOCO, the combined rate of alkene oxidation by O₃ and NO₃
764 was highest at night during summer.

765 Calculation of rates of instantaneous production of HO₂ from reactions of O₃ and NO₃ with
766 alkenes, using measurements made during the flights, has revealed that nighttime production
767 was dominated by NO₃ in summer and by O₃ in winter. The rate of instantaneous production
768 of HO₂ from reactions of NO₃ with alkenes decreased significantly from summer to winter
769 (87 %), whereas production from O₃ + alkene reactions was similar in summer and winter,
770 decreasing by just 31 %. Strong positive correlation between HO₂* and NO₃, especially
771 during flight B537, is attributed to the production of HO₂ from reactions of NO₃ with alkenes,
772 particularly *trans*-2-butene and other isomers of butene.

773 Significant concentrations of HO₂* were detected at night, with the highest HO₂*
774 concentration (13.6 pptv) being measured during a summer nighttime flight, indicating that
775 HO_x radical chemistry remains active at night under the right conditions. The role of HO_x is
776 diminished in the low photolysis winter daytime atmosphere, with alkene ozonolysis being
777 primarily responsible for oxidation and radical initiation, in agreement with previous studies
778 (e.g. Heard et al., 2004; Emmerson et al., 2005). Both the analysis presented here and the
779 results of the box modelling study by Stone et al. (2014b) indicate that in air masses removed
780 from sources of NO, NO₃ plays an important role in the oxidation of alkenes and radical
781 initiation at night, in agreement with previous studies (e.g. Brown et al., 2011). Alkene

782 ozonolysis also plays a significant role in nocturnal oxidation in agreement with Salisbury et
783 al. (2001), Geyer et al. (2003), [Ren et al. \(2003a\)](#), [Emmerson et al. \(2005\)](#), [Ren et al. \(2006\)](#),
784 [and Volkamer et al. \(2010\)](#) and others. The balance between the roles of NO₃ and O₃ was
785 controlled in part by [NO₃], with colder winter temperatures forcing the NO₃-N₂O₅
786 equilibrium towards N₂O₅.

787 The total rate of reaction of O₃ and NO₃ with alkenes during nighttime summer flights ($1.4 \times$
788 10^5 molecule cm⁻³ s⁻¹) was higher than during daytime winter flights (6.6×10^4 molecule
789 cm⁻³ s⁻¹) by a factor of 2.1. Whilst it should be remembered that measurements at different
790 times of day and in different seasons reflect composition changes in air masses (such as the
791 abundance of reactive alkenes) this result supports the hypothesis that oxidation of certain
792 VOCs, in particular the reactive alkenes, in the nocturnal summer atmosphere can be as rapid
793 as in the winter daytime atmosphere.

794 A box model of nighttime chemistry constrained to measurements of long lived species has
795 been used to investigate the nighttime chemistry sampled during RONOCO (Stone et al.,
796 2014b). The base model underpredicts HO₂* and overpredicts NO₃. These discrepancies were
797 minimised by increasing the concentration of alkenes in the model, thereby increasing
798 reaction of NO₃ with alkenes, and production of HO₂. The presence of unquantified
799 unsaturated VOCs has been confirmed by 2D-GC analysis, though the exact nature and
800 concentrations of the 'missing' species is unclear. The inclusion of these species in the
801 analysis presented in this paper would likely increase the role of NO₃ for oxidation of alkenes
802 and production of HO₂ at night.

803

804 **Acknowledgements**

805 This work was funded by the UK Natural Environment Research Council (NE/F004664/1).
806 The authors would like to thank ground staff, engineers, scientists and pilots involved in
807 RONOCO for making this project a success. Airborne data were obtained using the BAe 146-
808 301 Atmospheric Research Aircraft (ARA) flown by Directflight Ltd. and managed by the
809 Facility for Airborne Atmospheric Measurements (FAAM), which is a joint entity of the
810 Natural Environment Research Council (NERC) and the Met Office.

811

Comment [HW17]: See Reviewers'
Comments Sect. 2.10

1 **References**

- 2 Andrés-Hernández, M. D., Kartal, D., Crowley, J. N., Sinha, V., Regelin, E., Martínez-
3 Harder, M., Nenakhov, V., Williams, J., Harder, H., Bozem, H., Song, W., Thieser, J., Tang,
4 M. J., Hosaynali Beigi, Z., and Burrows, J. P.: Diel peroxy radicals in a semi-industrial
5 coastal area: nighttime formation of free radicals, *Atmospheric Chemistry and Physics*, 13,
6 5731-5749, 2013.
- 7 Atkinson, R., and Arey, J.: Gas-phase tropospheric chemistry of biogenic volatile organic
8 compounds: a review, *Atmospheric Environment*, 37, 197-219, 2003.
- 9 Beames, J. M., Liu, F., Lu, L., and Lester, M. I.: Ultraviolet Spectrum and Photochemistry of
10 the Simplest Criegee Intermediate CH_2OO , *Journal of the American Chemical Society*, 134,
11 20045-20048, 2012.
- 12 Beames, J. M., Liu, F., Lu, L., and Lester, M. I.: UV spectroscopic characterization of an
13 alkyl substituted Criegee intermediate CH_3CHOO , *Journal of Chemical Physics*, 138, 244307,
14 doi:10.1063/1.4810865, 2013.
- 15 Berndt, T., and Böge, O.: Kinetics of Oxirane Formation in the Reaction of Nitrate Radicals
16 with Tetramethylethylene, *Berichte der Bunsengesellschaft für physikalische Chemie*, 98,
17 869-871, 1994.
- 18 Bey, I., Aumont, B., and Toupance, G.: A modeling study of the nighttime radical chemistry
19 in the lower continental troposphere, *Journal of Geophysical Research: Atmospheres*, 106,
20 9991-10001, 2001.
- 21 Bloss, C., Wagner, V., Bonzanini, A., Jenkin, M. E., Wirtz, K., Martin-Reviejo, M., and
22 Pilling, M. J.: Evaluation of detailed aromatic mechanisms (MCMv3 and MCMv3.1) against
23 environmental chamber data, *Atmospheric Chemistry and Physics*, 5, 623-639, 2005.
- 24 Brown, S. S., and Stutz, J.: Nighttime radical observations and chemistry, *Chemical Society*
25 *Reviews*, 41, 6405-6447, 2012.
- 26 Brown, S. S., Dibb, J. E., Stark, H., Aldener, M., Vozella, M., Whitlow, S., Williams, E. J.,
27 Lerner, B. M., Jakoubek, R., Middlebrook, A. M., DeGouw, J. A., Warneke, C., Goldan, P.
28 D., Kuster, W. C., Angevine, W. M., Sueper, D. T., Quinn, P. K., Bates, T. S., Meagher, J. F.,
29 Fehsenfeld, F. C., and Ravishankara, A. R.: Nighttime removal of NO_x in the summer marine
30 boundary layer, *Geophysical Research Letters*, 31, L07108-L07113, 2004.

31 Brown, S. S., Osthoff, H. D., Stark, H., Dubé, W. P., Ryerson, T. B., Warneke, C., de Gouw,
32 J. A., Wollny, A. G., Parrish, D. D., Fehsenfeld, F. C., Ravishankara, A. R.: Aircraft
33 observations of daytime NO₃ and N₂O₅ and their implications for tropospheric chemistry,
34 *Journal of Photochemistry and Photobiology A: Chemistry*, 176, 270-278, 2005.

35 Brown, S. S., Ryerson, T. B., Wollny, A. G., Brock, C. A., Peltier, R., Sullivan, A. P., Weber,
36 R. J., Dubé, W. P., Trainer, M., Meagher, J. F., Fehsenfeld, F. C., and Ravishankara, A. R.:
37 Variability in Nocturnal Nitrogen Oxide Processing and Its Role in Regional Air Quality,
38 *Science*, 311, 67-70, 2006.

39 Brown, S. S., Dubé, W. P., Peischl, J., Ryerson, T., Atlas, E., Warneke, C., de Gouw, J. A., te
40 Lintel Hekkert, S., Brock, C. A., Flocke, F., Trainer, M., Parrish, D. D., Fehsenfeld, F. C., and
41 Ravishankara, A.: Budgets for nocturnal VOC oxidation by nitrate radicals aloft during the
42 2006 Texas Air Quality Study, *Journal of Geophysical Research: Atmospheres*, 116, D24305-
43 D24320, 2011.

44 Cantrell, C. A., Zimmer, A., and Tyndall, G. S.: Absorption cross sections for water vapor
45 from 183 to 193 nm, *Geophysical Research Letters*, 24, 2195-2198, 1997.

46 Carter, W. P. L., and Atkinson, R.: Alkyl Nitrate Formation from the Atmospheric
47 Photooxidation of Alkanes; a Revised Estimation Method, *Journal of Atmospheric Chemistry*,
48 8, 165-173, 1989.

49 Commane, R.: Understanding Radical Chemistry Throughout the Troposphere using Laser-
50 Induced Fluorescence Spectroscopy, PhD, Chemistry, University of Leeds, Leeds, 2009.

51 Commane, R., Floquet, C. F. A., Ingham, T., Stone, D., Evans, M. J., and Heard, D. E.:
52 Observations of OH and HO₂ radicals over West Africa, *Atmospheric Chemistry and Physics*,
53 10, 8783-8801, 2010.

54 Creasey, D. J., Halford-Maw, P. A., Heard, D. E., Pilling, M. J., and Whitaker, B. J.:
55 Implementation and initial deployment of a field instrument for measurement of OH and HO₂
56 in the troposphere by laser-induced fluorescence, *J. Chem. Soc.-Faraday Trans.*, 93, 2907-
57 2913, 1997.

58 Creasey, D. J., Heard, D. E., and Lee, J. D.: Eastern Atlantic Spring Experiment 1997
59 (EASE97) 1. Measurements of OH and HO₂ concentrations at Mace Head, Ireland, *Journal of*
60 *Geophysical Research: Atmospheres*, 107, 4091-4106, 2002.

61 Dari-Salisburgo, C., Di Carlo, P., Giammaria, F., Kajji, Y., and D'Altorio, A.: Laser induced
62 fluorescence instrument for NO₂ measurements: Observations at a central Italy background
63 site, *Atmospheric Environment*, 43, 970-977, 2009.

64 Di Carlo, P., Aruffo, E., Busilacchio, M., Giammaria, F., Dari-Salisburgo, C., Biancofiore, F.,
65 Visconti, G., Lee, J., Moller, S., Reeves, C. E., Baugitte, S., Forster, G., Jones, R. L., and
66 Ouyang, B.: Aircraft based four-channel thermal dissociation laser induced fluorescence
67 instrument for simultaneous measurements of NO₂, total peroxy nitrate, total alkyl nitrate, and
68 HNO₃, *Atmospheric Measurement Techniques*, 6, 971-980, 2013.

69 Donahue, N. M., Kroll, J. H., Anderson, J. G., and Demerjian, K. L.: Direct observation of
70 OH production from the ozonolysis of olefins, *Geophysical Research Letters*, 25, 59-62, 1998.

71 Donahue, N. M., Drozd, G. T., Epstein, S. A., Presto, A. A., and Kroll, J. H.: Adventures in
72 ozoneland: down the rabbit-hole, *Physical Chemistry Chemical Physics*, 13, 10848-10857,
73 2011.

74 Drozd, G. T., and Donahue, N. M.: Pressure Dependence of Stabilized Criegee Intermediate
75 Formation from a Sequence of Alkenes, *Journal of Physical Chemistry A*, 115, 4381-4387,
76 2011.

77 Dusanter, S., Vimal, D., Stevens, P. S., Volkamer, R., and Molina, L. T.: Measurements of
78 OH and HO₂ concentrations during the MCMA-2006 field campaign - Part 1: Deployment of
79 the Indiana University laser-induced fluorescence instrument, *Atmospheric Chemistry and
80 Physics*, 9, 1665-1685, 2009.

81 Edwards, G. D., Cantrell, C., Stephens, S., Hill, B., Goyea, O., Shetter, R., Mauldin, R. L.,
82 Kosciuch, E., Tanner, D., and Eisele, F.: Chemical Ionization Mass Spectrometer Instrument
83 for the Measurement of Tropospheric HO₂ and RO₂, *Analytical Chemistry*, 75, 5317-5327,
84 2003.

85 Emmerson, K. M., and Carslaw, N.: Night-time radical chemistry during the TORCH
86 campaign, *Atmospheric Environment*, 43, 3220-3226, 2009.

87 Emmerson, K. M., and Evans, M. J.: Comparison of tropospheric gas-phase chemistry
88 schemes for use within global models, *Atmospheric Chemistry and Physics*, 9, 1831-1845,
89 2009.

90 Emmerson, K. M., Carslaw, N., and Pilling, M. J.: Urban Atmospheric Chemistry During the
91 PUMA Campaign 2: Radical Budgets for OH, HO₂ and RO₂, *Journal of Atmospheric*
92 *Chemistry*, 52, 165-183, 2005.

93 Emmerson, K. M., Carslaw, N., Carslaw, D. C., Lee, J. D., McFiggans, G., Bloss, W. J.,
94 Gravestock, T., Heard, D. E., Hopkins, J., Ingham, T., Pilling, M. J., Smith, S. C., Jacob, M.,
95 and Monks, P. S.: Free radical modelling studies during the UK TORCH Campaign in
96 Summer 2003, *Atmospheric Chemistry and Physics*, 7, 167-181, 2007.

97 Faloon, I. C., Tan, D., Leshner, R. L., Hazen, N. L., Frame, C. L., Simpas, J. B., Harder, H.,
98 Martinez, M., di Carlo, P., Ren, X., and Brune, W. H.: A Laser-Induced Fluorescence
99 Instrument for Detecting Tropospheric OH and HO₂: Characteristics and Calibration, *Journal*
100 *of Atmospheric Chemistry*, 47, 139-167, 2004.

101 Fleming, Z. L., Monks, P. S., Rickard, A. R., Heard, D. E., Bloss, W. J., Seakins, P. W., Still,
102 T. J., Sommariva, R., Pilling, M. J., Morgan, R., Green, T. J., Brough, N., Mills, G. P.,
103 Penkett, S. A., Lewis, A. C., Lee, J. D., Saiz-Lopez, A., and Plane, J. M. C.: Peroxy radical
104 chemistry and the control of ozone photochemistry at Mace Head, Ireland during the summer
105 of 2002, *Atmospheric Chemistry and Physics*, 6, 2193-2214, 2006.

106 Floquet, C. F. A.: Airborne Measurements of Hydroxyl Radicals by Fluorescence Assay by
107 Gas Expansion, PhD, School of Chemistry, University of Leeds, Leeds, 155 pp., 2006.

108 Fuchs, H., Bohn, B., Hofzumahaus, A., Holland, F., Lu, K. D., Nehr, S., Rohrer, F., and
109 Wahner, A.: Detection of HO₂ by laser-induced fluorescence: Calibration and interferences
110 from RO₂ radicals, *Atmospheric Measurement Techniques*, 4, 1255-1302, 2011.

111 Gerbig, C., Schmitgen, S., Kley, D., and Volz-Thomas, A.: An improved fast-response
112 vacuum-UV resonance fluorescence CO instrument, *Journal of Geophysical Research:*
113 *Atmospheres*, 104, 1699-1704, 1999.

114 German, K. R.: Direct measurement of the radiative lifetimes of the $A^2\Sigma^+$ ($V'=0$), *Journal of*
115 *Chemical Physics*, 62, 2584-2587, 1975.

116 Geyer, A., and Stutz, J.: The vertical structure of OH-HO₂-RO₂ chemistry in the nocturnal
117 boundary layer: A one-dimensional model study, *Journal of Geophysical Research:*
118 *Atmospheres*, 109, D16301-D16316, 2004a.

119 Geyer, A., and Stutz, J.: Vertical profiles of NO₃, N₂O₅, O₃, and NO_x in the nocturnal
120 boundary layer: 2. Model studies on the altitude dependence of composition and chemistry,
121 Journal of Geophysical Research: Atmospheres, 109, D12307, doi:10.1029/2003JD004211,
122 2004b.

123 Geyer, A., Bächmann, K., Hofzumahaus, A., Holland, F., Konrad, S., Klüpfel, T., Pätz, H.-
124 W., Perner, D., Mihelcic, D., Schäfer, H.-J., Volz-Thomas, A., and Platt, U.: Nighttime
125 formation of peroxy and hydroxyl radicals during the BERLIOZ campaign: Observations and
126 modeling studies, Journal of Geophysical Research: Atmospheres, 108, 8249-8263, 2003.

127 Harrison, R. M., Yin, J., Tilling, R. M., Cai, X., Seakins, P. W., Hopkins, J. R., Lansley, D.
128 L., Lewis, A. C., Hunter, M. C., Heard, D. E., Carpenter, L. J., Creasey, D. J., Lee, J. D.,
129 Pilling, M. J., Carslaw, N., Emmerson, K. M., Redington, A., Derwent, R. G., Ryall, D.,
130 Mills, G., and Penkett, S. A.: Measurement and modelling of air pollution and atmospheric
131 chemistry in the U.K. West Midlands conurbation: Overview of the PUMA Consortium
132 project, Science of the Total Environment, 360, 5-25, 2006.

133 Heard, D. E.: Atmospheric field measurements of the hydroxyl radical using laser-induced
134 fluorescence spectroscopy, Annual Review of Physical Chemistry, 57, 191–216, 2006.

135 Heard, D. E., Carpenter, L. J., Creasey, D. J., Hopkins, J. R., Lee, J. D., Lewis, A. C., Pilling,
136 M. J., Seakins, P. W., Carslaw, N., and Emmerson, K. M.: High levels of the hydroxyl radical
137 in the winter urban troposphere, Geophysical Research Letters, 31, L18112-L18117,
138 10.1029/2004gl020544, 2004.

139 Hewitt, C. N., Lee, J. D., MacKenzie, A. R., Barkley, M. P., Carslaw, N., Carver, G. D.,
140 Chappell, N. A., Coe, H., Collier, C., Commane, R., Davies, F., Davison, B., Di Carlo, P., Di
141 Marco, C. F., Dorsey, J. R., Edwards, P. M., Evans, M. J., Fowler, D., Furneaux, K. L.,
142 Gallagher, M., Guenther, A., Heard, D. E., Helfter, C., Hopkins, J., Ingham, T., Irwin, M.,
143 Jones, C., Karunaharan, A., Langford, B., Lewis, A. C., Lim, S. F., MacDonald, S. M.,
144 Mahajan, A. S., Malpass, S., McFiggans, G., Mills, G., Misztal, P., Moller, S., Monks, P. S.,
145 Nemitz, E., Nicolas-Perea, V., Oetjen, H., Oram, D. E., Palmer, P. I., Phillips, G. J., Pike, R.,
146 Plane, J. M. C., Pugh, T., Pyle, J. A., Reeves, C. E., Robinson, N. H., Stewart, D., Stone, D.,
147 Whalley, L. K., and Yin, X.: Overview: oxidant and particle photochemical processes above a
148 south-east Asian tropical rainforest (the OP3 project): introduction, rationale, location
149 characteristics and tools, Atmospheric Chemistry and Physics, 10, 169-199, 2010.

150 Holland, F., Hofzumahaus, A., Schäfer, J., Kraus, A., and Pätz, H.-W.: Measurements of OH
151 and HO₂ radical concentrations and photolysis frequencies during BERLIOZ, Journal of
152 Geophysical Research: Atmospheres, 108, 8246-8261, 2003.

153 Hopkins, J. R., Lewis, A. C., and Read, K. A.: A two-column method for long-term
154 monitoring of non-methane hydrocarbons (NMHCs) and oxygenated volatile organic
155 compounds (*o*-VOCs), Journal of Environmental Monitoring, 5, 8-13, 2003.

156 Jenkin, M. E., Saunders, S. M., and Pilling, M. J.: The tropospheric degradation of volatile
157 organic compounds: A protocol for mechanism development, Atmospheric Environment, 31,
158 81-104, 1997.

159 Jenkin, M. E., Saunders, S. M., Wagner, V., and Pilling, M. J.: Protocol for the development
160 of the Master Chemical Mechanism, MCM v3 (Part B): tropospheric degradation of aromatic
161 volatile organic compounds, Atmospheric Chemistry and Physics, 3, 181-193, 2003.

162 Johnson, D., and Marston, G.: The gas-phase ozonolysis of unsaturated volatile organic
163 compounds in the troposphere, Chemical Society Reviews, 37, 699-716, 2008.

164 Jones, A. R., Thomson, D. J., Hort, M., and Devenish, B.: The U.K. Met Office's next-
165 generation atmospheric dispersion model, NAME III, in: Air Pollution Modeling and its
166 Application XVII (Proceedings of the 27th NATO/CCMS International Technical Meeting on
167 Air Pollution Modelling and its Application), edited by: Borrego, C., and Norman, A.-L.,
168 Springer, Dordrecht, Netherlands, 580-589, 2007.

169 Kanaya, Y., Sadanaga, Y., Matsumoto, J., Sharma, U. K., Hirokawa, J., Kajii, Y., and
170 Akimoto, H.: Nighttime observation of the HO₂ radical by an LIF instrument at Oki Island,
171 Japan, and its possible origins, Geophysical Research Letters, 26, 2179-2182, 1999.

172 Kennedy, O. J., Ouyang, B., Langridge, J. M., Daniels, M. J. S., Baugitte, S., Freshwater, R.,
173 McLeod, M. W., Ironmonger, C., Sendall, J., Norris, O., Nightingale, R., Ball, S. M., and
174 Jones, R. L.: An aircraft based three channel broadband cavity enhanced absorption
175 spectrometer for simultaneous measurements of NO₃, N₂O₅ and NO₂, Atmospheric
176 Measurement Techniques, 4, 1759-1776, 2011.

177 Kroll, J. H., Clarke, J. S., Donahue, N. M., Anderson, J. G., and Demerjian, K. L.: Mechanism
178 of HO_x Formation in the Gas-Phase Ozone-Alkene reaction. 1. Direct, Pressure-Dependent
179 Measurements of Prompt OH Yields, J. Phys. Chem. A, 105, 1554-1560, 2001a.

180 Kroll, J. H., Sahay, S. R., Anderson, J. G., Demerjian, K. L., and Donahue, N. M.:
181 Mechanism of HO_x Formation in the Gas-Phase Ozone-Alkene Reaction. 2. Prompt versus
182 Thermal Dissociation of Carbonyl Oxides to Form OH, *Journal of Physical Chemistry A*,
183 105, 4446-4457 2001b.

184 Kroll, J. H., Donahue, N. M., Cee, V. J., Demerjian, K. L., and Anderson, J. G.: Gas-Phase
185 Ozonolysis of Alkenes: Formation of OH from Anti Carbonyl Oxides, *Journal of the*
186 *American Chemical Society*, 124, 8518-8519, 2002.

187 Lee, J. D., Lewis, A. C., Monks, P. S., Jacob, M., Hamilton, J. F., Hopkins, J. R., Watson, N.
188 M., Saxton, J. E., Ennis, C., Carpenter, L. J., Carslaw, N., Fleming, Z. L., Bandy, A., Oram,
189 D. E., Penkett, S. A., Slemr, J., Norton, E. G., Rickard, A. R., Whalley, L. K., Heard, D. E.,
190 Bloss, W. J., Gravestock, T., Smith, S. C., Stanton, J., Pilling, M. J., and Jenkin, M. E.: Ozone
191 photochemistry and elevated isoprene during the UK heatwave of August 2003, *Atmospheric*
192 *Environment*, 40, 7598– 7613, 2006.

193 Lidster, R. T., Hamilton, J. F., Lee, J. D., Lewis, A. C., Hopkins, J. R., Punjabi, S., Rickard,
194 A. R., and Young, J. C.: The impact of monoaromatic hydrocarbons on OH reactivity in the
195 coastal UK boundary layer and free troposphere, *Atmospheric Chemistry and Physics*, 14,
196 6677-6693, 2014.

197 Lightfoot, P. D., Cox, R. A., Crowley, J. N., Destriau, M., Hayman, G. D., Jenkin, M. E.,
198 Moortgat, G. K., and Zabel, F.: Organic Peroxy Radicals: Kinetics, Spectroscopy and
199 Tropospheric Chemistry, *Atmospheric Environment*, 26A, 1805-1961, 1992.

200 Lou, S., Holland, F., Rohrer, F., Lu, K., Bohn, B., Brauers, T., Chang, C. C., Fuchs, H.,
201 Häsel, R., Kita, K., Kondo, Y., Li, X., Shao, M., Zeng, L., Wahner, A., Zhang, Y., Wang,
202 W., and Hofzumahaus, A.: Atmospheric OH reactivities in the Pearl River Delta - China in
203 summer 2006: measurement and model results, *Atmospheric Chemistry and Physics*, 10,
204 11243-11260, 10.5194/acp-10-11243, 2010.

205 Lu, K. D., Rohrer, F., Holland, F., Fuchs, H., Bohn, B., Brauers, T., Chang, C. C., Häsel, R.,
206 Hu, M., Kita, K., Kondo, Y., Li, X., Lou, S. R., Nehr, S., Shao, M., Zeng, L. M., Wahner, A.,
207 Zhang, Y. H., and Hofzumahaus, A.: Observation and modelling of OH and HO₂
208 concentrations in the Pearl River Delta 2006: a missing OH source in a VOC rich atmosphere,
209 *Atmospheric Chemistry and Physics*, 12, 1541-1569, 2012.

210 Lu, K. D., Hofzumahaus, A., Holland, F., Bohn, B., Brauers, T., Fuchs, H., Hu, M., Häsel, R.,
211 R., Kita, K., Kondo, Y., Li, X., Lou, S. R., Oebel, A., Shao, M., Zeng, L. M., Wahner, A.,
212 Zhu, T., Zhang, Y. H., and Rohrer, F.: Missing OH source in a suburban environment near
213 Beijing: observed and modelled OH and HO₂ concentrations in summer 2006, *Atmospheric
214 Chemistry and Physics*, 13, 1057-1080, 2013.

215 Lu, K., Rohrer, F., Holland, F., Fuchs, H., Brauers, T., Oebel, A., Dlugi, R., Hu, M., Li, X.,
216 Lou, S., Shao, M., Zhu, T., Wahner, A., Zhang, Y., and Hofzumahaus, A.: Nighttime
217 observation and chemistry of HO_x in the Pearl River Delta and Beijing in summer 2006,
218 *Atmospheric Chemistry and Physics*, 14, 4979-4999, doi:10.5194/acp-14-4979-2014, 2014.

219 Martinez, M., Harder, H., Kubistin, D., Rudolf, M., Bozem, H., Eerdekens, G., Fischer, H.,
220 Klüpfel, T., Gurk, C., Königstedt, R., Parchatka, U., Schiller, C. L., Stickler, A., Williams, J.,
221 and Lelieveld, J.: Hydroxyl radicals in the tropical troposphere over the Suriname rainforest:
222 airborne measurements, *Atmospheric Chemistry and Physics*, 10, 3759-3773, 10.5194/acp-10-
223 3759, 2010.

224 Mauldin III, R. L., Berndt, T., Sipilä, M., Paasonen, P., Petäjä, T., Kim, S., Kurtén, A.,
225 Stratmann, F., Kerminen, V.-M., and Kulmala, M.: A new atmospherically relevant oxidant of
226 sulphur dioxide, *Nature*, 488, 193-196, 2012.

227 Morgan, W. T., Ouyang, B., Allan, B. J., Aruffo, E., Di Carlo, P., Kennedy, O. J., Lowe, D.,
228 Flynn, M. J., Rosenberg, P. D., Williams, P. I., Jones, R., McFiggans, G. B., and Coe, H.:
229 Influence of aerosol chemical composition on N₂O₅ uptake: airborne regional measurements
230 in North-Western Europe, *Atmospheric Chemistry and Physics Discussions*, 14, 19673-
231 19718, 2014.

232 Nakajima, M., and Endo, Y.: Determination of the molecular structure of the simplest Criegee
233 intermediate CH₂OO, *Journal of Chemical Physics*, 139, 101103, doi:10.1063/1.4821165,
234 2013.

235 Nakajima, M., and Endo, Y.: Spectroscopic characterization of an alkyl substituted Criegee
236 intermediate *syn*-CH₃CHOO through pure rotational transitions, *Journal of Chemical Physics*,
237 140, 011101, doi:10.1063/1.4861494, 2014.

238 Ouyang, B., McLeod, M. W., Jones, R. L., and Bloss, W. J.: NO₃ radical production from the
239 reaction between the Criegee intermediate CH₂OO and NO₂, *Physical Chemistry Chemical
240 Physics*, 15, 17070-17075, 2013.

241 Paulson, S. E., and Orlando, J. J.: The reactions of ozone with alkenes: An important source
242 of HO_x in the boundary layer, *Geophysical Research Letters*, 23, 3727-3730, 1996.

243 Ren, X., Harder, H., Martinez, M., Leshner, R., Oligier, A., Simpas, J. B., Brune, W. H.,
244 Schwab, J. J., Demerjian, K. L., He, Y., Zhou, X., and Gao, H.: OH and HO₂ chemistry in the
245 urban atmosphere of New York City, *Atmospheric Environment*, 37, 3639-3651, 2003a.

246 Ren, X., Harder, H., Martinez, M., Leshner, R. L., Oligier, A., Shirley, T., Adams, J., Simpas, J.
247 B., and Brune, W. H.: HO_x concentrations and OH reactivity observations in New York City
248 during PMTACS-NY2001, *Atmospheric Environment*, 37, 3627-3637, 2003b.

249 Ren, X., Brune, W. H., Mao, J., Mitchell, M. J., Leshner, R., Simpas, J. B., Metcalf, A. R.,
250 Schwab, J. J., Cai, C., Li, Y., Demerjian, K. L., Felton, H. D., Boynton, G., Adams, A., Perry,
251 J., He, Y., Zhou, X., and Hou, J.: Behavior of OH and HO₂ in the winter atmosphere in New
252 York City, *Atmospheric Environment*, 40, 252-263, 2006.

253 Salisbury, G., Rickard, A. R., Monks, P. S., Allan, B. J., Bauguutte, S. J. B., Penkett, S. A.,
254 Carslaw, N., Lewis, A. C., Creasey, D. J., Heard, D. E., Jacobs, P. J., and Lee, J. D.:
255 Production of peroxy radicals at night via reactions of ozone and the nitrate radical in the
256 marine boundary layer, *Journal of Geophysical Research: Atmospheres*, 106, 12669-12687,
257 2001.

258 Saunders, S. M., Jenkin, M. E., Derwent, R. G., and Pilling, M. J.: Protocol for the
259 development of the Master Chemical Mechanism, MCM v3 (Part A): tropospheric
260 degradation of non-aromatic volatile organic compounds, *Atmospheric Chemistry and
261 Physics*, 3, 161-180, 2003.

262 Sheehy, P. M., Volkamer, R., Molina, L. T., and Molina, M. J.: Oxidative capacity of the
263 Mexico City atmosphere - Part 2: A RO_x radical cycling perspective, *Atmospheric Chemistry
264 and Physics*, 10, 6993-7008, 2010.

265 Shirley, T. R., Brune, W. H., Ren, X., Mao, J., Leshner, R., Cardenas, B., Volkamer, R.,
266 Molina, L. T., Molina, M. J., Lamb, B., Velasco, E., Jobson, T., and Alexander, M.:
267 Atmospheric oxidation in the Mexico City Metropolitan Area (MCMA) during April 2003,
268 *Atmospheric Chemistry and Physics*, 6, 2753-2765, 2006.

269 Smith, S. C., Lee, J. D., Bloss, W. J., Johnson, G. P., Ingham, T., and Heard, D. E.:
270 Concentrations of OH and HO₂ radicals during NAMBLEX: measurements and steady state
271 analysis, *Atmospheric Chemistry and Physics*, 6, 1435-1453, 2006.

272 Sommariva, R., Pilling, M. J., Bloss, W. J., Heard, D. E., Lee, J. D., Fleming, Z. L., Monks,
273 P. S., Plane, J. M. C., Saiz-Lopez, A., Ball, S. M., Bitter, M., Jones, R. L., Brough, N.,
274 Penkett, S. A., Hopkins, J. R., Lewis, A. C., and Read, K. A.: Night-time radical chemistry
275 during the NAMBLEX campaign, *Atmospheric Chemistry and Physics*, 7, 587-598, 2007.

276 Sommariva, R., Osthoff, H. D., Brown, S. S., Bates, T. S., Baynard, T., Coffman, D., de
277 Gouw, J. A., Goldan, P. D., Kuster, W. C., Lerner, B. M., Stark, H., Warneke, C., Williams,
278 E. J., Fehsenfeld, F. C., Ravishankara, A. R., and Trainer, M.: Radicals in the marine
279 boundary layer during NEAQS 2004: a model study of day-time and night-time sources and
280 sinks, *Atmospheric Chemistry and Physics*, 9, 3075-3093, 2009.

281 Stewart, D. J., Taylor, C. M., Reeves, C. E., and McQuaid, J.: Biogenic nitrogen oxide
282 emissions from soils: impact on NO_x and ozone over west Africa during AMMA (African
283 Monsoon Multidisciplinary Analysis): observational study, *Atmospheric Chemistry and
284 Physics*, 8, 2285-2297, 2008.

285 Still, T. J., Al-Haider, S., Seakins, P. W., Sommariva, R., Stanton, J. C., Mills, G., and
286 Penkett, S. A.: Ambient formaldehyde measurements made at a remote marine boundary layer
287 site during the NAMBLEX campaign - a comparison of data from chromatographic and
288 modified Hantzsch techniques., *Atmospheric Chemistry and Physics*, 6, 2711-2726, 2006.

289 Stone, D., Evans, M. J., Commane, R., Ingham, T., Floquet, C. F. A., McQuaid, J. B.,
290 Brookes, D. M., Monks, P. S., Purvis, R., Hamilton, J. F., Hopkins, J., Lee, J., Lewis, A. C.,
291 Stewart, D., Murphy, J. G., Mills, G., Oram, D., Reeves, C. E., and Heard, D. E.: HO_x
292 observations over West Africa during AMMA: impact of isoprene and NO_x, *Atmospheric
293 Chemistry and Physics*, 10, 9415-9429, 2010.

294 Stone, D., Whalley, L. K., and Heard, D. E.: Tropospheric OH and HO₂ radicals: field
295 measurements and model comparisons, *Chemical Society Reviews*, 41, 6348-6404, 2012.

296 Stone, D., Blitz, M., Daubney, L., Howes, N. U. M., and Seakins, P.: Kinetics of CH₂OO
297 reactions with SO₂, NO₂, NO, H₂O and CH₃CHO as a function of pressure, *Physical
298 Chemistry Chemical Physics*, 16, 1139-1149, 2014a.

299 Stone, D., Evans, M. J., Walker, H. M., Ingham, T., Vaughan, S., Ouyang, B., Kennedy, O. J.,
300 McLeod, M. W., Jones, R. L., Hopkins, J., Punjabi, S., Lidster, R., Hamilton, J. F., Lee, J. D.,
301 Lewis, A. C., Carpenter, L. J., Forster, G., Oram, D., Reeves, C. E., Baugitte, S., Morgan, W.,
302 Coe, H., Aruffo, E., Dari-Salisburgo, C., Giammaria, F., Di Carlo, P., and Heard, D. E.:
303 Radical chemistry at night: comparisons between observed and modelled HO_x, NO₃ and N₂O₅
304 during the RONOCO project, *Atmospheric Chemistry and Physics*, 14, 1299-1321, 2014b.

305 Stutz, J., Alicke, B., Ackermann, R., Geyer, A., White, A., and Williams, E.: Vertical profiles
306 of NO₃, N₂O₅, O₃, and NO_x in the nocturnal boundary layer: 1. Observations during the Texas
307 Air Quality Study 2000, *Journal of Geophysical Research: Atmospheres*, 109, D12306-
308 D12320, 2004.

309 Su, Y.-T., Huang, Y.-H., Witek, H. A., and Lee, Y.-P.: Infrared Absorption Spectrum of the
310 Simplest Criegee Intermediate CH₂OO, *Science*, 340, 174-176, 2013.

311 Taatjes, C. A., Meloni, G., Selby, T. M., Trevitt, A. J., Osborn, D. L., Percival, C. J., and
312 Shallcross, D. E.: Direct Observation of the Gas-Phase Criegee Intermediate (CH₂OO),
313 *Journal of the American Chemical Society*, 130, 11883-11885, 2008.

314 Taatjes, C. A., Welz, O., Eskola, A. J., Savee, J. D., Osborn, D. L., Lee, E. P. F., Dyke, J. M.,
315 Mok, D. W. K., Shallcross, D. E., and Percival, C. J.: Direct measurement of Criegee
316 intermediate (CH₂OO) reactions with acetone, acetaldehyde, and hexafluoroacetone, *Physical
317 Chemistry Chemical Physics*, 14, 10391-10400, 2012.

318 Taatjes, C. A., Welz, O., Eskola, A. J., Savee, J. D., Scheer, A. M., Shallcross, D. E.,
319 Rotavera, B., Lee, E. P. F., Dyke, J. M., Mok, D. W. K., Osborn, D. L., and Percival, C. J.:
320 Direct Measurements of Conformer-Dependent Reactivity of the Criegee Intermediate
321 CH₃CHOO, *Science*, 340, 177-180, 2013.

322 Taatjes, C. A., Shallcross, D. E., and Percival, C. J.: Research frontiers in the chemistry of
323 Criegee intermediates and tropospheric ozonolysis, *Physical Chemistry Chemical Physics*, 16,
324 1689-2180, 2014.

325 Vereecken, L., and Francisco, J. S.: Theoretical studies of atmospheric reaction mechanisms
326 in the troposphere, *Chemical Society Reviews*, 41, 6217-6708, 2012.

327 Volkamer, R., Sheehy, P., Molina, L. T., and Molina, M. J.: Oxidative capacity of the Mexico
328 City atmosphere - Part 1: A radical source perspective, *Atmospheric Chemistry and Physics*,
329 10, 6969-6991, 2010.

330 Welz, O., Savee, J. D., Osborn, D. L., Vasu, S. S., Percival, C. J., Shallcross, D. E., and
331 Taatjes, C. A.: Direct Kinetic Measurements of Criegee Intermediate (CH_2OO) Formed by
332 Reaction of CH_2I with O_2 , *Science*, 335, 204-207, 2012.

333 Whalley, L. K., Furneaux, K. L., Goddard, A., Lee, J. D., Mahajan, A., Oetjen, H., Read, K.
334 A., Kaaden, N., Carpenter, L. J., Lewis, A. C., Plane, J. M. C., Saltzman, E. S., Wiedensohler,
335 A., and Heard, D. E.: The chemistry of OH and HO_2 radicals in the boundary layer over the
336 tropical Atlantic Ocean, *Atmospheric Chemistry and Physics*, 10, 1555-1576, 2010.

337 Whalley, L. K., Blitz, M. A., Desservettaz, M., Seakins, P. W., and Heard, D. E.: Reporting
338 the sensitivity of Laser Induced Fluorescence instruments used for HO_2 detection to an
339 interference from RO_2 radicals and introducing a novel approach that enables HO_2 and certain
340 RO_2 types to be selectively measured, *Atmospheric Measurement Techniques*, 6, 3425-3440,
341 2013.

342 Winiberg, F. A. F., Smith, S. C., Bejan, I., Brumby, C. A., Ingham, T., Malkin, T. L., Orr, S.
343 C., Heard, D. E., and Seakins, P. W.: Pressure dependent calibration of the OH and HO_x
344 channels of a FAGE HO_x instrument using the Highly Instrumented Reactor for Atmospheric
345 Chemistry (HIRAC), *Atmospheric Measurement Techniques Discussions*, 7, 7963-8011,
346 2014.

347 Wong, K. W., and Stutz, J.: Influence of nocturnal vertical stability on daytime chemistry: A
348 one-dimensional model study, *Atmospheric Environment*, 44, 3753-3760, 2010.

1 Table 1. Examples of modelling studies and observations of HO_x radicals and VOC oxidation at night. PERCA = Peroxy Radical Chemical
 2 Amplification; LIF = Laser Induced Fluorescence; DOAS = Differential Optical Absorption Spectroscopy; MCM = Master Chemical Mechanism;
 3 MIESR = Matrix Isolation Electron Spin Resonance; RACM = Regional Atmospheric Chemistry Mechanism; CRDS = Cavity Ring Down
 4 Spectroscopy; CIMS = Chemical Ionisation Mass Spectrometry; GC = Gas Chromatography; PTRMS = Proton Transfer Reaction Mass Spectrometry;
 5 FTIR = Fourier Transform Infrared Spectroscopy; DUALER (DUAL channel peroxy radical chemical amplifier); OA-CRD = Off Axis Cavity Ring
 6 Down Spectroscopy; CRM-PTR-MS = Comparative Reactivity Method Proton Transfer Mass Spectrometry.

Location, Campaign, Date	Methods	Results	Reference
Mace Head, Ireland, EASE97, 1997	Measurements: [HO ₂ +RO ₂] measured by PERCA; HO _x measured by LIF; NO ₃ measured by DOAS). Modelling: Campaign-tailored box model constrained to measurements, based on MCM.	2 nights of HO _x measurements: HO ₂ = 1–2 and 0.5–0.7 pptv; OH not detected above limit of detection ($\sim 2.5 \times 10^5 \text{ cm}^{-3}$). NO ₃ dominated radical production in westerly (clean) air masses; O ₃ dominated in NE, SE, and SW air masses and dominated radical production overall during the campaign.	Salisbury et al. (2001); Creasey et al. (2002)
Pabstthum, Germany, BERLIOZ 1998,	Measurements: HO _x measured by LIF; NO ₃ measured by DOAS and MIESR. Modelling: Zero-dimensional model using lumped VOC reactivity, constrained to measured species.	Nighttime OH = $1.85 \times 10^5 \text{ cm}^{-3}$, compared to modelled value of $4.1 \times 10^5 \text{ cm}^{-3}$. Nighttime HO ₂ = $3 \times 10^7 \text{ cm}^{-3}$, model results in agreement. NO ₃ chemistry responsible for 53 % of HO ₂ and 36 % of OH during the night. O ₃ + alkene responsible for 47 % of HO ₂ and 64 % of OH during the night.	Geyer et al. (2003); Holland et al. (2003)
Birmingham, PUMA, 1999 and 2000	Measurements: HO _x measured by LIF. Modelling: Photochemical box model constrained to measurements, based on MCM.	Daytime OH initiation dominated by O ₃ + alkenes, HONO photolysis, and O(¹ D) + H ₂ O during summer. O ₃ + alkenes dominated in winter. O ₃ + alkenes main radical source at night.	Emmerson et al. (2005); Harrison et al. (2006)
New York, PMTACS-NY, 2001	Measurements: HO _x measured by LIF.	Nighttime OH $\sim 7 \times 10^5 \text{ cm}^{-3}$ and nighttime HO ₂ $\sim 8 \times 10^6 \text{ cm}^{-3}$. Increase in HO _x after midnight attributed to increase in O ₃ due to transport. O ₃ + alkenes main source of nighttime HO _x .	Ren et al. (2003a); Ren et al. (2003b)

Mace Head, NAMBLEX, 2002	Measurements: HO _x measured by LIF; NO ₃ measured by DOAS. Modelling: Zero-dimensional box models constrained to measured species, based on MCM.	Nighttime HO ₂ = 2–3 × 10 ⁷ cm ⁻³ ; OH below detection limit (6 × 10 ⁴ cm ⁻³). Model overestimated HO ₂ . On average, O ₃ + alkene reactions contributed 59 % and NO ₃ + alkene reactions contributed 41 % to RO ₂ production at night, but NO ₃ and RO ₂ concentrations were always higher in semi-polluted air masses than in clean marine air masses and NO ₃ reactions dominated in these conditions.	Fleming et al. (2006); Smith et al. (2006); Sommariva et al. (2007)
Writtle, London, TORCH, 2003	Measurements: HO _x measured by LIF, RO ₂ measured by PERCA, during a heatwave/pollution episode. Modelling: zero-dimensional box model constrained to measured species.	OH and HO ₂ observed above the limit of detection on several nights. OH peaked at 8.5 × 10 ⁵ cm ⁻³ ; HO ₂ peaked at 1 × 10 ⁸ cm ⁻³ . Model overpredicted nighttime OH and HO ₂ on average by 24 % and 7 %; underpredicted [HO ₂ +ΣRO ₂] by 22 %.	Lee et al. (2006); Emmerson et al. (2007); Emmerson and Carslaw (2009)
Mexico City, MCMA 2003	Measurements: HO _x measured by LIF, NO ₃ measured by DOAS. Modelling: Zero-dimensional model based on MCM v3.1, constrained to measured species.	Polluted city location characterized by high levels of NO, NO ₂ and O ₃ . Maximum nighttime OH ~ 1 × 10 ⁶ cm ⁻³ ; maximum nighttime HO ₂ ~ 6 pptv. Nighttime production of radicals dominated by O ₃ + alkene reactions (76–92 %); NO ₃ + alkene plays a minor role. Daytime radical production ~ 25 times higher than night.	Shirley et al. (2006); Sheehy et al. (2010); Volkamer et al. (2010)
New York City, PMTACS-NY winter 2004	Measurements: HO _x measured by LIF. Modelling: Zero-dimensional model based on RACM and constrained by measurements.	Mean maximum OH = 0.05 pptv; mean maximum HO ₂ = 0.7 pptv. Model under-prediction of HO ₂ was pronounced when NO was high. O ₃ + alkene reactions were dominant nighttime source.	Ren et al. (2006)
Gulf of Maine, Northeast United States, NEAQS, 2004	Measurements: NO ₃ and N ₂ O ₅ measured by CRDS. Modelling: Zero-dimensional model based on MCM v3.1, constrained to measured species. No measurements of OH, HO ₂ , or RO ₂ .	Ship-based measurements onboard <i>RV Ronald H. Brown</i> in the Gulf of Maine, influenced by unpolluted marine air masses and polluted air masses from USA and Canada. Maximum modelled nighttime HO ₂ = 7.0 × 10 ⁸ cm ⁻³ . Base model overestimated NO ₃ and NO ₂ observations by 30–50 %. In anthropogenic air masses reaction with VOCs and RO ₂ each accounted for 40 % of modelled NO ₃ loss.	Sommariva et al. (2009)
Houston, Texas, TexAQS, 2006	Measurements: NO ₃ and N ₂ O ₅ measured by CRDS, VOCs measured by CIMS, GC, and PTRMS. No direct measurements of OH, HO ₂ ,	Loss rates and budgets of NO ₃ and highly reactive VOCs calculated. NO ₃ primarily lost through reaction with VOCs. VOC oxidation dominated by NO ₃ , which was 3–5 times more important than O ₃ .	Brown et al. (2011)

or RO₂.

Pearl River Delta, China, PRIDE-PRD, 2006	Measurements: HO _x measured by LIF; OH reactivity measured by laser-flash photolysis and LIF; VOCs measured by FTIR and GC. Modelling: Box model based on RACM and the Mainz Isoprene Mechanism, and constrained by measurements.	Rural site 60 km downwind of large urban region (Guangzhou), with low local wind speeds favouring accumulation of air pollutants. Maximum nighttime OH (hourly average) = $5 \times 10^6 \text{ cm}^{-3}$; maximum nighttime HO ₂ (hourly average) = $1 \times 10^9 \text{ cm}^{-3}$. Unknown recycling mechanism required for the model to reproduce measured nighttime values. OH reactivity peaked at night. Missing nighttime reactivity attributed to unmeasured secondary organic compounds.	Lou et al. (2010); Lu et al. (2012); Lu et al. (2013)
Beijing, CAREBEIJIN G2006, 2006	Measurements: HO _x measured by LIF; OH lifetime measured by laser flash photolysis and LIF; VOCs measured by GC. Modelling: Box model based on RACM and the Mainz Isoprene Mechanism, and constrained by measurements.	Suburban rural site south of Beijing, under the influence of slowly moving, aged polluted air from the south. OH reactivity peaked at night. Model generally underestimated observed nighttime OH concentrations.	Lu et al. (2013); Lu et al. (2014)
Cape Verde, RHaMBLE, 2007	Measurements: HO _x measured by LIF. Modelling: Box model based on MCM with added halogen chemistry scheme, constrained to measurements of long-lived species.	Clean tropical Atlantic measurement site with occasional continental influence. OH was not measured at night. HO ₂ was detected on two nights, up to $2.5 \times 10^7 \text{ cm}^{-3}$. Model underprediction of HO ₂ was significantly reduced by constraining the model to 100 pptv of peroxy acetyl nitrate (PAN) at night.	Whalley et al. (2010)
Huelva, Spain, DOMINO, 2008	Measurements: [HO ₂ +RO ₂] measured by DUALER; HO _x measured by LIF; NO ₃ and N ₂ O ₅ measured by OA-CRD; OH reactivity measured by CRM-PTR-MS. No measurements of anthropogenic VOCs.	Coastal forested site with strong urban-industrial and weak biogenic influences. Maxima in [HO ₂ +RO ₂] and [HO ₂] were observed around noon and midnight. Enhanced nighttime [HO ₂ +RO ₂] (up to 80 pptv) was observed in air masses from the urban-industrial region. Maximum nighttime HO ₂ = 8 pptv. Measured NO ₃ was generally below LOD; calculated NO ₃ up to 20 pptv. Calculated production of RO ₂ from NO ₃ +alkenes accounts for 47–54 % of observed [HO ₂ +RO ₂]. Ozonolysis of unmeasured alkenes could account for remaining [HO ₂ +RO ₂].	Andrés-Hernández et al. (2009)

7 Table 2. Details of supporting measurements.

Species	Instrument, Technique	Time resolution; Limit of detection (LOD)	References
CO	Aero Laser AL5002 Fast Carbon Monoxide Monitor. Excitation and fast response fluorescence at $\lambda = 150$ nm.	1 s; 3.5 ppbv	Gerbig et al. (1999)
O ₃	Thermo Scientific TEi49C Ozone analyser. Absorption spectroscopy at $\lambda = 254$ nm.	1 s; 0.6 ppbv	Hewitt et al. (2010)
NO, NO ₂ , NO _x (NO + NO ₂)	Air Quality Design dual channel fast-response NO _x instrument. Chemiluminescence from NO + O ₃ reaction. Conversion of NO ₂ to NO by photolysis.	10 s; 3 pptv for NO, 15 pptv for NO ₂	Stewart et al. (2008)
NO ₂ , Σ ANs, Σ PNs	TD-LIF (thermal dissociation laser induced fluorescence). Detection of NO ₂ by laser-induced fluorescence. Thermal decomposition of Σ ANs (total alkyl nitrate) and Σ PNs (total peroxy nitrate) to NO ₂ .	1 s; 9.8 pptv for NO ₂ , 28.1 pptv for Σ ANs, 18.4 pptv for Σ PNs	Dari-Salisburgo et al. (2009); Di Carlo et al. (2013)
Alkenes	Whole air samples (WAS) analysed by laboratory-based gas chromatography with flame ionization detection (GC-FID).	Typically 30 s; variable limits of detection	Hopkins et al. (2003)
NO ₃ , N ₂ O ₅	BBCEAS (broadband cavity-enhanced absorption spectroscopy) of NO ₃ at $\lambda = 642$ – 672 nm. N ₂ O ₅ measured following thermal dissociation to NO ₃ + NO ₂ .	1 s; 1.1 pptv for NO ₃ , 2.4 pptv for NO ₃ + N ₂ O ₅	Kennedy et al. (2011)
HCHO	Hantzsch technique: Liquid-phase reaction of formaldehyde followed by excitation, and fluorescence of resulting adduct at $\lambda = 510$ nm.	60 s; 81 pptv	Still et al. (2006)

8 Table 3. Mean mixing ratios of selected gas phase species, and air temperature, measured during
 9 RONOCO and SeptEx. The flight and season during which the maximum values were measured
 10 are given in parentheses. NO₂ data are from the TD-LIF instrument. Zero values indicate
 11 measurements below the limit of detection.

Species	Summer RONOCO	SeptEx	Winter RONOCO	Maximum
CO / ppbv	102.3	117.1	139.3	256.0 (B537, summer)
O ₃ / ppbv	39.6	40.4	38.6	89.8 (B537, summer)
NO ₃ / pptv	21.1	0	6.2	176.9 (B537, summer)
NO / ppbv	0.05	0	0	18.9 (B539, summer)
NO ₂ / ppbv	1.6	1.7	2.3	18.6 (B568, winter)
Temperature / K	286.5	286.2	276.4	297.5 (B537, summer)

12 Table 4. Combined daytime and nighttime mean concentrations of OH and mean mixing ratios of
 13 HO₂* with the FAGE instrument's average 1σ limits of detection for a 5 minute averaging period
 14 during the RONOCO and SeptEx fieldwork.

Comment [HW18]: See Reviewers' Comments Sect 1.3

	OH / molecule cm ⁻³		HO ₂ * / pptv	
	Mean concentration	Limit of detection	Mean mixing ratio	Limit of detection
Summer		1.8 × 10 ⁶	1.6	0.03
SeptEx	1.8 × 10 ⁶	1.2 × 10 ⁶	2.9	0.02
Winter		6.4 × 10 ⁵	0.7	0.02

15 | Table 5. Mean and, in parentheses, maximum HO₂* mixing ratios measured during RONOCO
16 | and SeptEx.

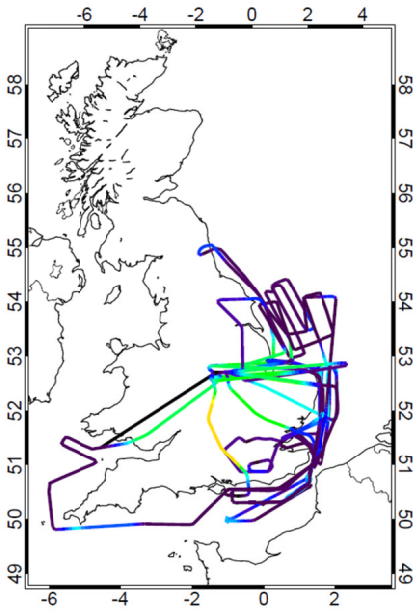
	Mean (maximum) HO ₂ * mixing ratio / pptv		
	Summer	SeptEx	Winter
Dawn	0.74 (1.19)		0.54 (1.81)
Day		3.78 (11.79)	0.49 (1.68)
Dusk	2.73 (9.97)		0.32 (0.97)
Night	1.86 (13.58)		0.98 (2.02)

17 | Table 6. Average Rates of instantaneous production of HO₂ from reactions of O₃ and NO₃ with
 18 | alkenes.

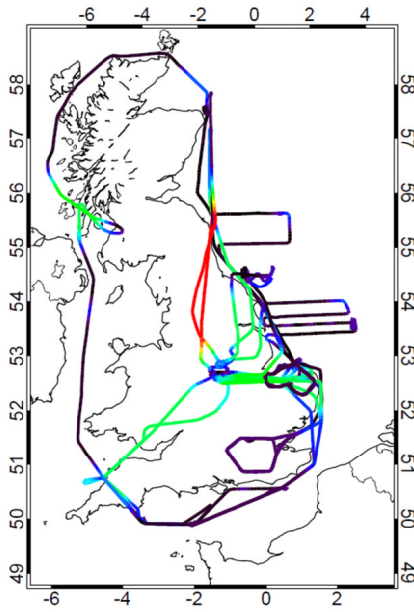
Comment [HW19]: See Reviewers' Comments Sect 1.4

Measurements	HO ₂ production rate (ΣP_{HO_2}) / 10 ⁴ molecule cm ⁻³ s ⁻¹			
	Dawn	Day	Dusk	Night
Summer				
NO ₃	0		2.8	3.8
O ₃	0.5		2.2	1.7
Total	0.5		5.0	5.5
Winter				
NO ₃	0.4	0.4	0.4	0.5
O ₃	1.4	1.5	1.2	1.2
Total	1.8	1.9	1.6	1.7

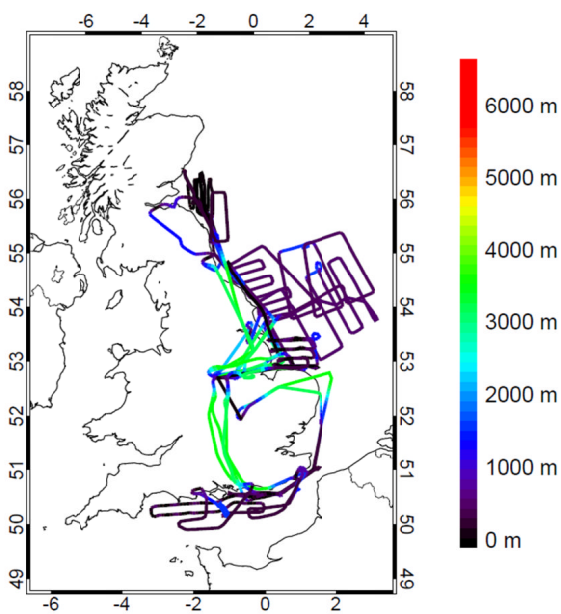
(a) Summer RONOCO



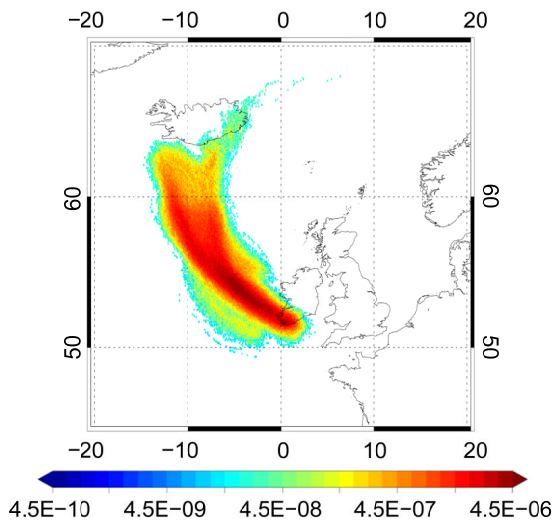
(b) SeptEx



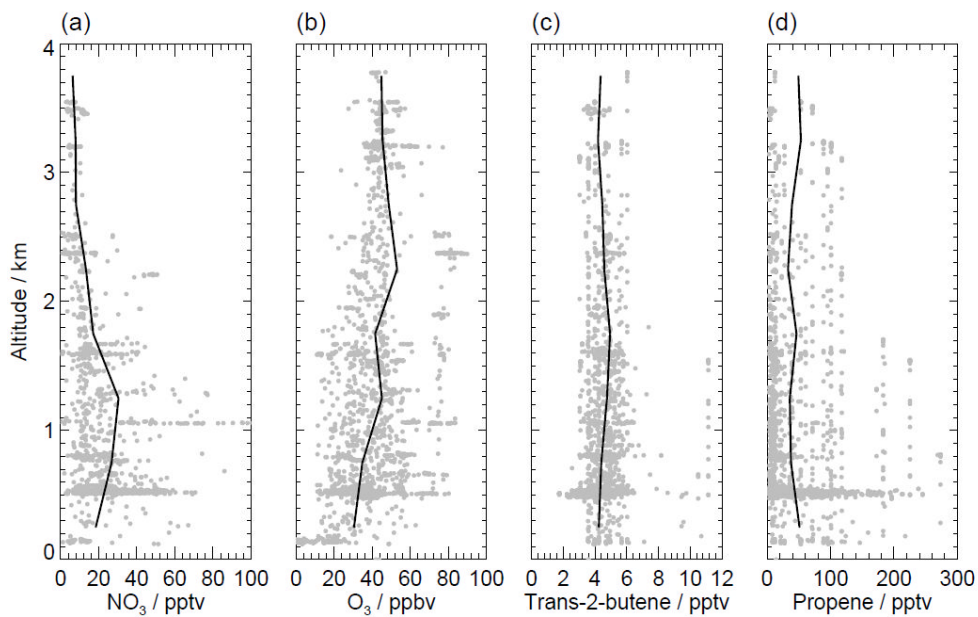
(c) Winter RONOCO



5
0 Figure 1. Flight paths for: (a) Summer RONOCO, (b) SeptEx, and (c) winter RONOCO
9 measurement campaigns, coloured by altitude.

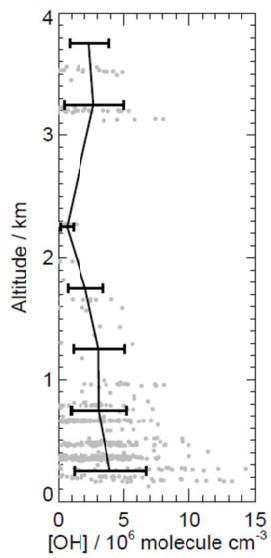


5
 14 Figure 2. Footprint map for flight B535 on 17th July 2010, showing model particle densities (g s m^{-3}) in a 300 m deep layer from the surface, integrated over a 24 hour period beginning 48
 15 hours prior to the flight.



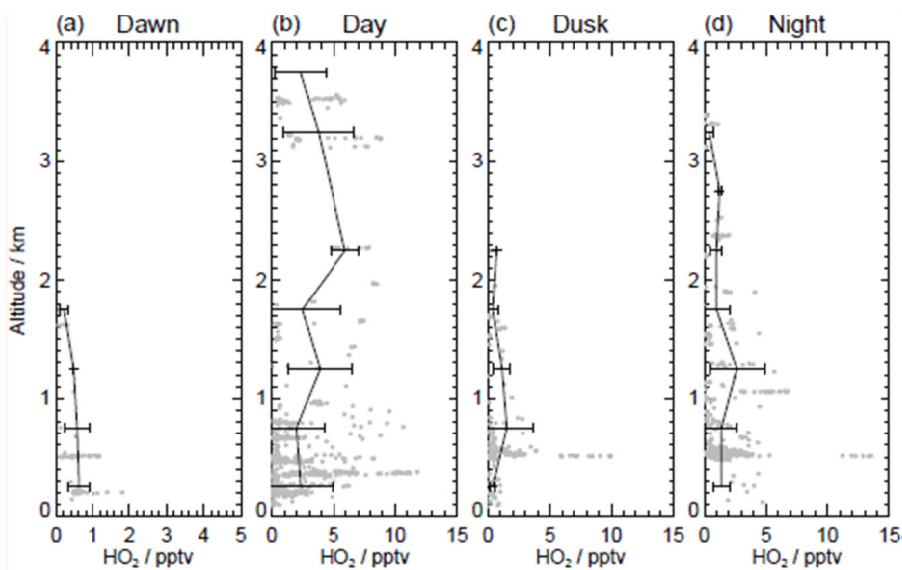
9
 14 Figure 3. Nighttime altitude profiles of a) NO_3 ; b) O_3 ; c) *trans*-2-butene; d) propene, showing
 15 60 second data (grey points) and mean values in 500 m altitude bins (solid black lines).

Comment [HW20]: See Reviewers' Comments Sect 1.4

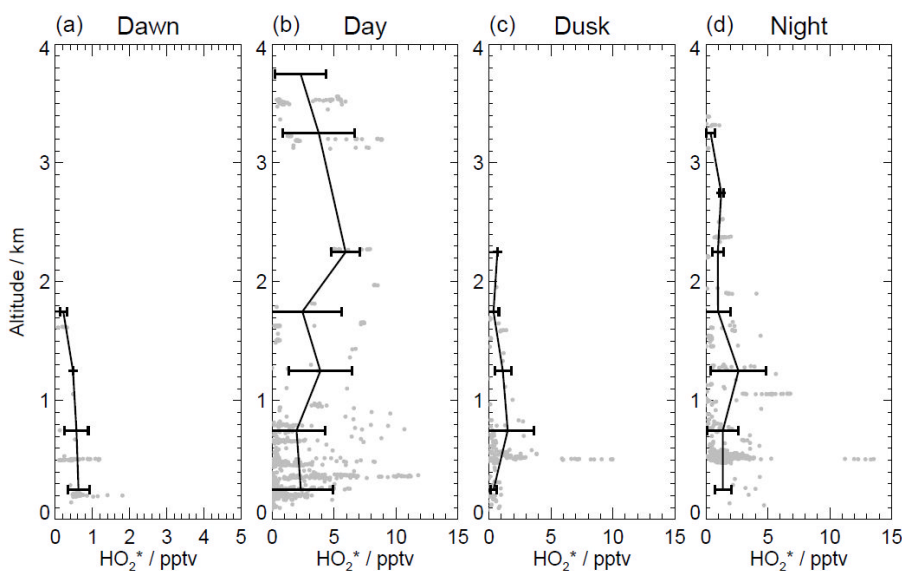


5
 0 Figure 43. Altitude profile of OH measured during SeptEx showing 60 second data (grey
 1 points) and mean values in 500 m altitude bins (solid black lines). Error bars are 1σ .

Formatted: Font: Not Italic



Comment [HW21]: Figure updated with HO₂*. See Reviewers' Comments Sect. 1.1.



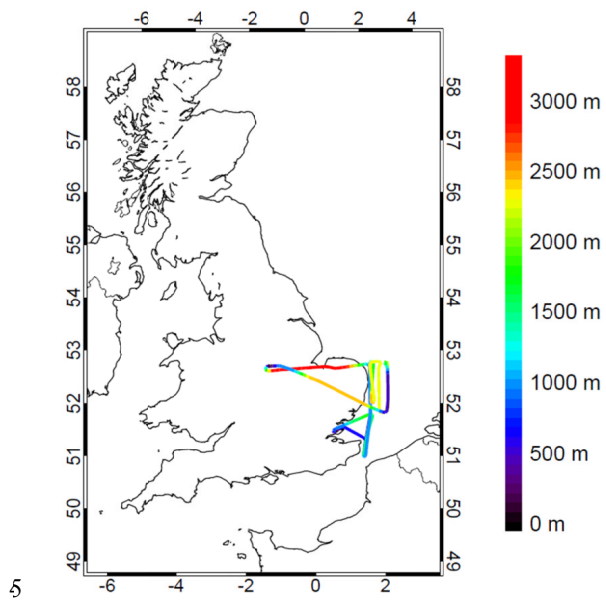
5

5

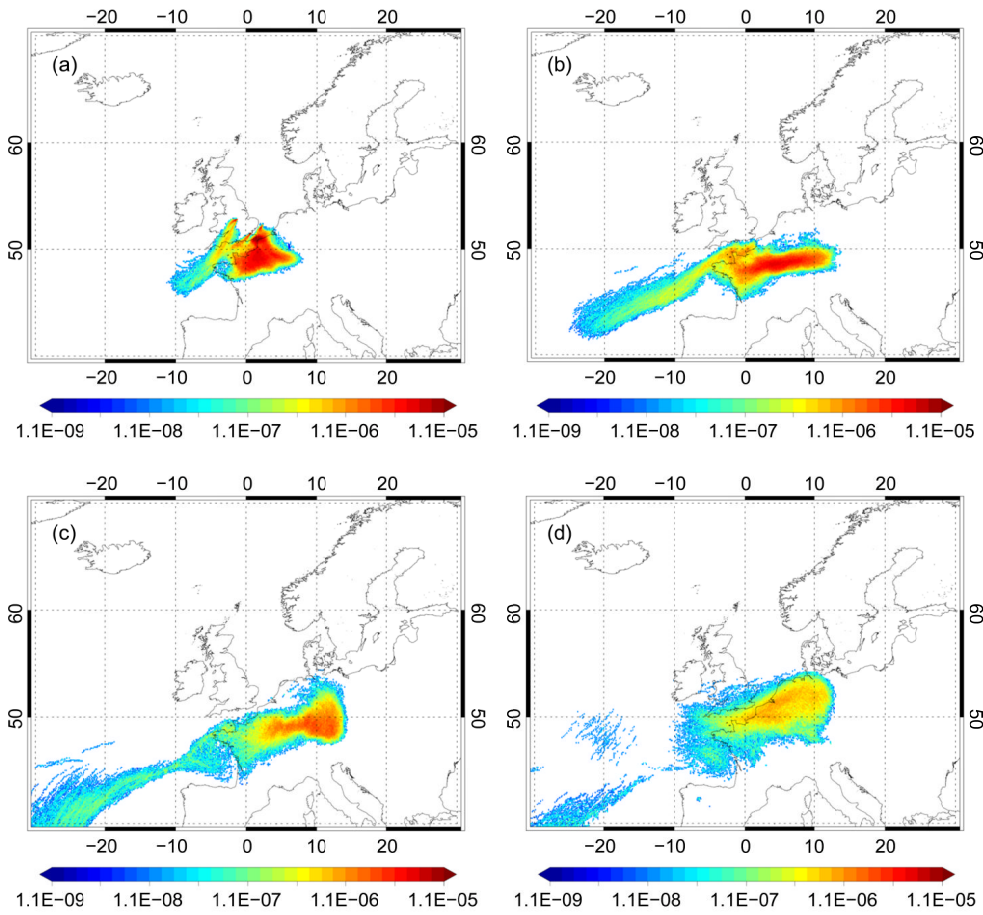
15 **Figure 54.** Altitude profiles of HO₂* measured in RONOCO and SeptEx during: a) dawn; b)
 15 day; c) dusk; d) night, showing 60 second data (grey points) and mean values in 500 m
 17 altitude bins (solid black lines). Error bars are 1σ.

Comment [HW22]: See Reviewers' Comments Sect. 1.1

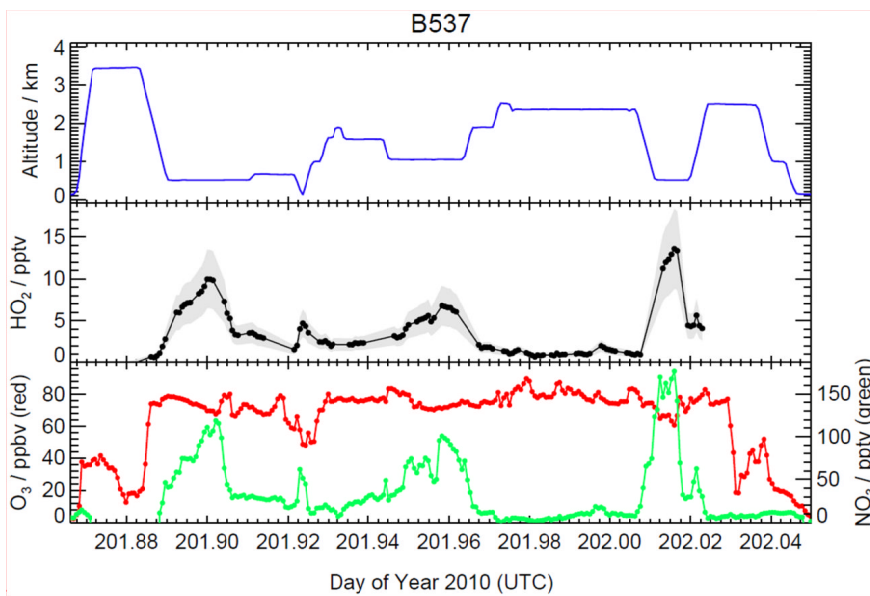
Formatted: Font: Not Italic



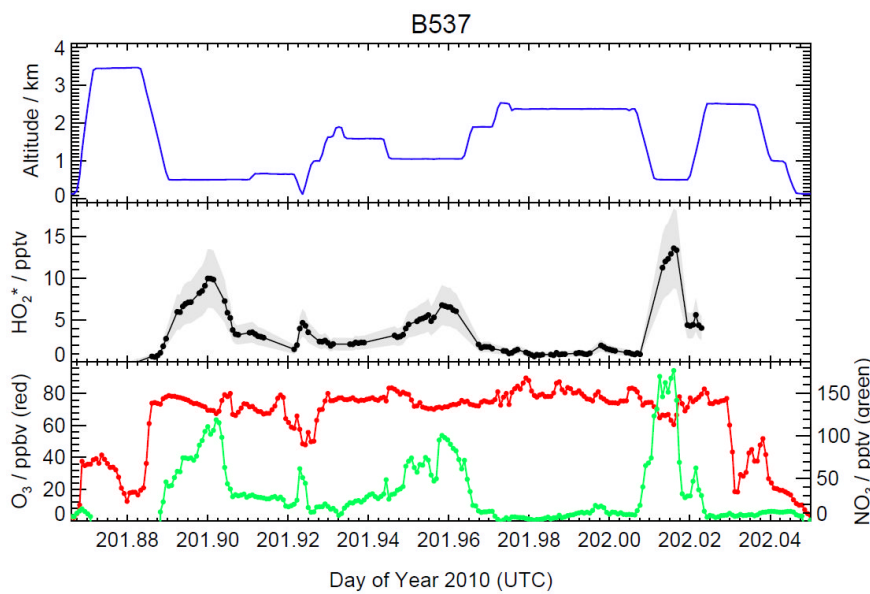
5 | Figure 65. Flight track of flight B537 on 20th July 2010, coloured by altitude.



5
 14 | Figure 76. Footprint maps for flight B537 on 20th July 2010, showing model particle densities
 15 (g s m^{-3}) in a 300 m deep layer from the surface, integrated over 24 hour periods beginning
 15 (a) 24 hours, (b) 48 hours, (c) 72 hours, and (d) 96 hours prior to the flight.

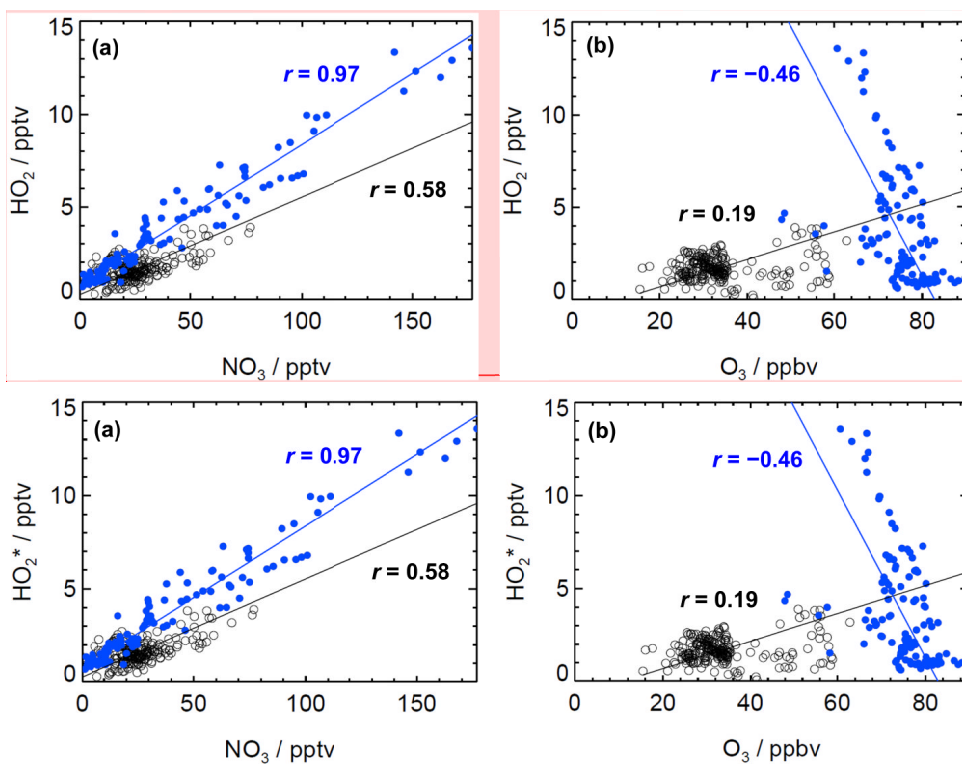


Comment [HW23]: Figure updated with HO₂*. See Reviewers' Comments Sect. 1.1.



Comment [HW24]: See Reviewers' Comments Sect. 1.1.

Figure 87. Time series of altitude (top panel, blue), HO₂* (middle panel, black, with grey shading representing the uncertainty in the measurements), O₃ (bottom panel, red) and NO₃ (bottom panel, green) during nighttime flight B537 on 20th July 2010.



Comment [HW25]: Figure updated with HO₂*. See Reviewers' Comments Sect. 1.1

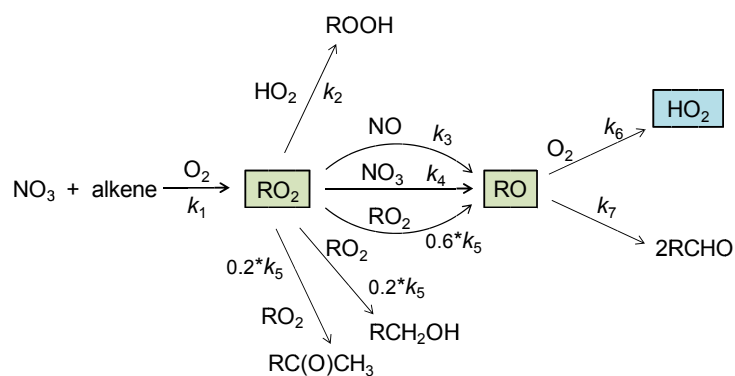
5

5

7

10 **Figure 98.** HO₂* versus (a) NO₃ and (b) O₃ during flight B537 (blue, filled circles) and during
 13 all other nighttime flights (black, open circles). The solid lines are lines of best fit to the data.

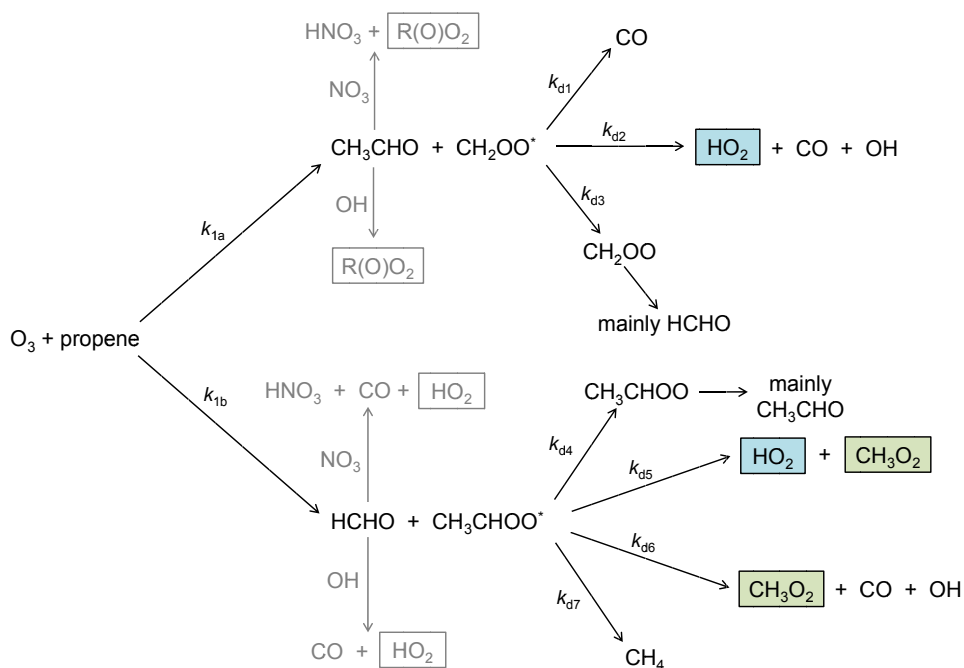
Comment [HW26]: See Reviewers' Comments Sect. 1.1



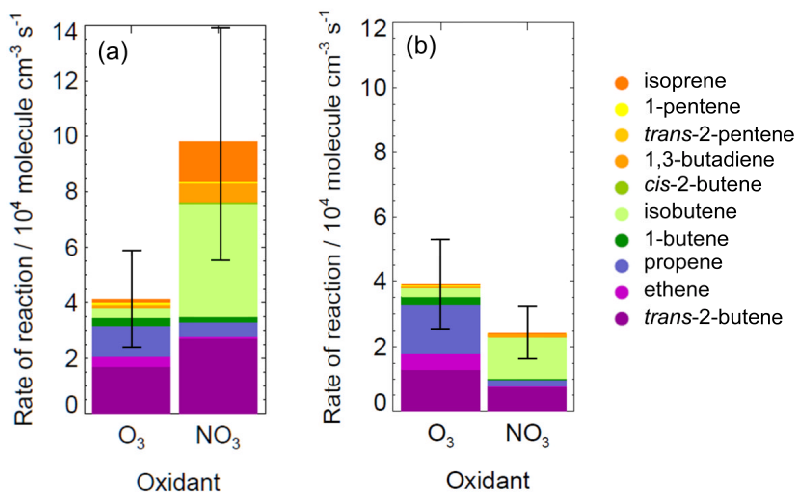
9

15 **Figure 109.** Generalised reaction scheme for production of RO₂ and HO₂ following reaction
 16 of NO₃ with an alkene.

13

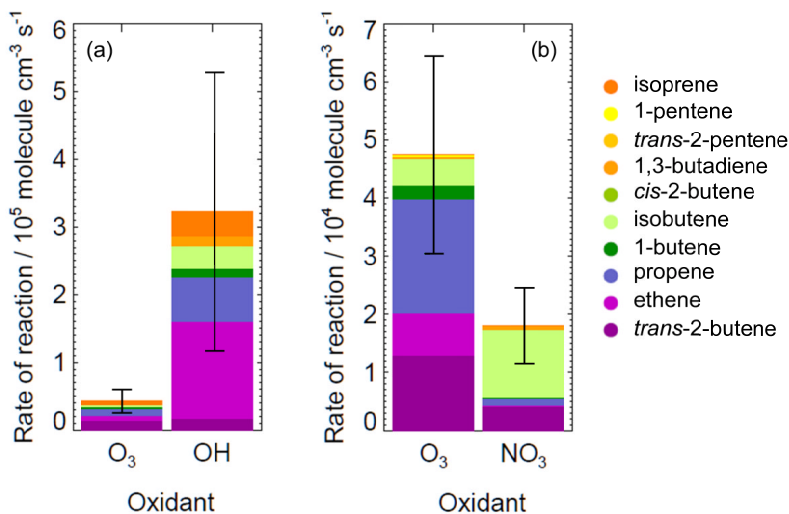


5
 0 Figure 11+0. Reaction scheme for $O_3 + \text{propene}$, showing production of HO_2 and the methyl
 9 peroxy radical, CH_3O_2 .



3
 17 Figure 12+1. Average Nighttime rates of reaction between O_3 and NO_3 with alkenes during:
 18 a) summer; and b) winter RONOCO flights. Error bars represent the combined uncertainty in
 10 the measurements.

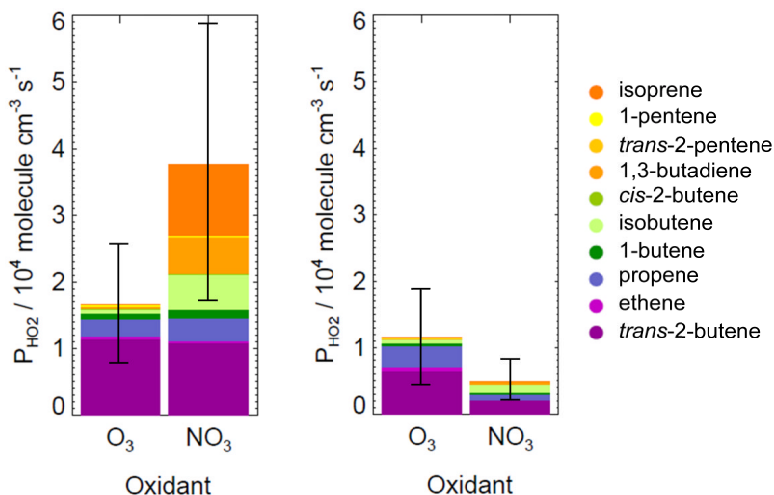
Comment [HW27]: See Reviewers' Comments Sect 1.4



5

12 Figure 1342. Average daytime rates of reaction of (a) O_3 and OH with alkenes during
 18 SeptEx; and (b) O_3 and NO_3 with alkenes during winter. Note the different scales. NO_3 was
 14 not detected during daytime SeptEx flights (LOD = 1.1pptv); OH was not detected during
 26 daytime winter flights (LOD = 6.4×10^5 molecule cm^{-3}). Error bars represent the combined
 25 uncertainties in the measurements.

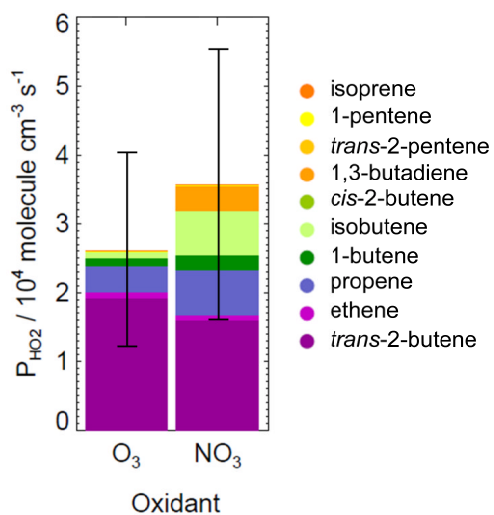
Comment [HW28]: See Reviewers' Comments Sect 1.4



10

10 Figure 1413. Averaged rates of instantaneous production of HO_2 from reactions of O_3 and
 11 NO_3 with alkenes during: a) summer; and b) winter RONOCO flights. Error bars represent the
 12 combined uncertainty in the measurements.

Comment [HW29]: See Reviewers' Comments Sect 1.4

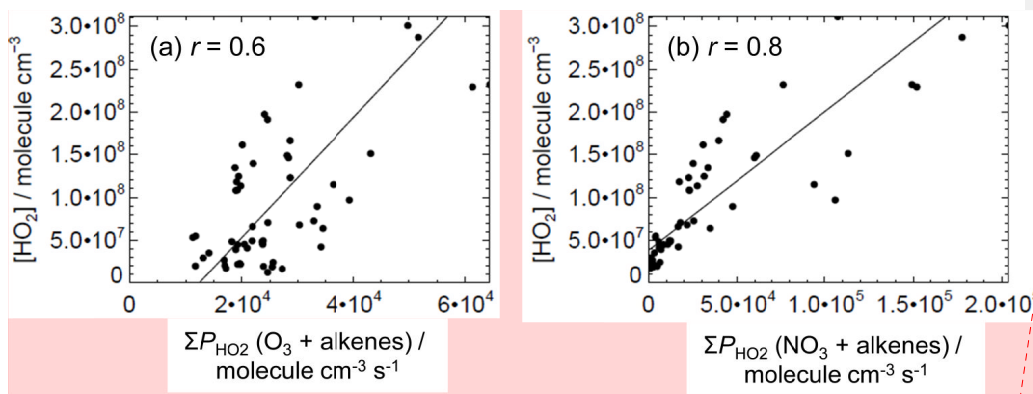


5

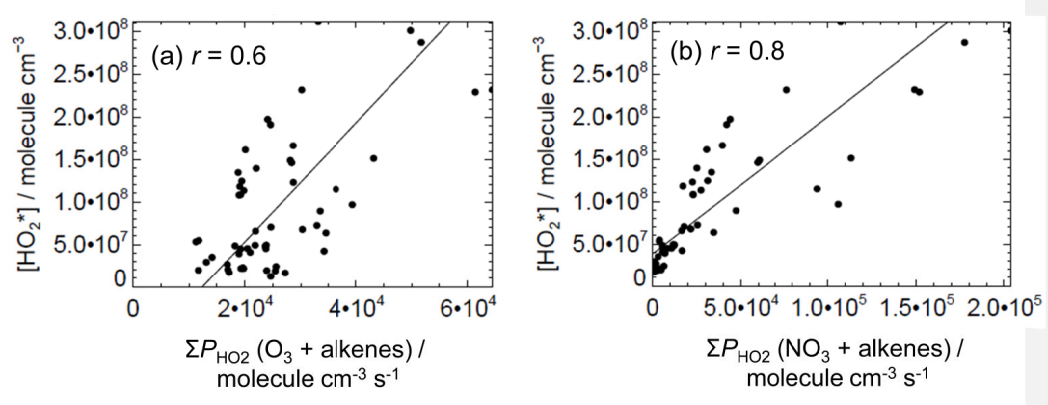
14 | Figure 15-14. Average Rates of instantaneous production of HO₂ (P_{HO_2}) from reactions of O₃
 15 | and NO₃ with alkenes during flight B537. Error bars represent the combined uncertainty in
 15 | the measurements.

9

Comment [HW30]: See Reviewers' Comments Sect 1.4



Comment [HW31]: Figure updated with 'HO2*'. See Reviewers' Comments Sect. 1.1



5

5

15 **Figure 1615.** $[HO_2^*]$ versus total rate of instantaneous production of HO_2 from reactions of:
 15 a) O_3 ; and b) NO_3 during flight B537. Correlation coefficients (r) are given in each plot. Solid
 17 lines are lines of best fit to the data.

Comment [HW32]: See Reviewers' Comments Sect. 1.1